Surface Buoyancy Forcing and the Mixed Layer of the Western Pacific Warm Pool: Observations and 1D Model Results*

STEVEN P. ANDERSON AND ROBERT A. WELLER

Department of Physical Oceanography, Woods Hole Oceanographic Institution, Woods Hole, Massachusetts

ROGER B. LUKAS

Department of Oceanography, University of Hawaii at Manoa, Honolulu, Hawaii

(Manuscript received 15 September 1995, in final form 26 March 1996)

ABSTRACT

The broad, shallow body of warm (>29°C) water found in the western tropical Pacific Ocean plays an important role in the coupled ocean–atmosphere dynamics and thermodynamics associated with the El Niño–Southern Oscillation phenomenon. Thus, it is important to understand the processes that maintain and perturb that warm pool. Measurements from a buoy moored in the center of the warm pool during the TOGA Coupled Ocean–Atmosphere Response Experiment show that the exchange of mass between the ocean and atmosphere is as important as the exchange of heat. Rain forms a shallow, buoyant layer that does not mix with the water below except during infrequent strong wind events. Using a one-dimensional mixed layer model, it is demonstrated that the rate of local precipitation governs the mixed layer depth and can thus alter the rates of change in sea surface temperature during both warming and cooling periods. The observed mixed layer depth in the warm pool is at a depth that allows for maximum warming by capturing a significant portion of the shortwave radiation, but is shallow enough to avoid entrainment cooling. Either increased rain rates or reduced wind forcing yields a shallow mixed layer, which may be associated with cooling of the sea surface temperature in spite of a net positive heat flux at the sea surface because penetrating shortwave radiation is lost across the base of the shallow, fresh mixed layer. Decreased rain rates or increased wind forcing can turn on entrainment cooling of the surface mixed layer.

1. Introduction

The warmest open ocean waters in the world are found in the western equatorial Pacific, where annual average upper-ocean temperatures can exceed 29°C over an area comparable in size to Australia (Fig. 1). This warm pool is closely associated with intense atmospheric convection and rainfall, which provide a major driving force for global atmospheric circulation. Eastward displacement of this coupled warm pool system during El Niño–Southern Oscillation events (Gill and Rasmusson 1983) results in pronounced midlatitude circulation anomalies (Palmer and Mansfield 1984). Understanding the processes that couple the ocean and atmosphere in the warm pool and are responsible for maintaining and perturbing this system is a crucial step toward improving our ability to predict seasonal-to-interannual climate variability. The pursuit of this understanding is the primary objective of the Tropical Oceans–Global Atmosphere (TOGA) Coupled Ocean–Atmosphere Response Experiment (COARE; Webster and Lukas 1992).

In this paper, we analyze the response of the mixed layer in the western Pacific warm pool to local surface forcing using observations made during TOGA COARE and a one-dimensional model of the upper-ocean response to local surface forcing. We examine the surface buoyancy forcing's role in determining the vertical structure of the near-surface waters of the warm pool and its net effect on sea surface temperature. Section 2 reviews the relevant ocean surface mixed layer processes. Section 3 describes the field experiment. Surface buoyancy forcing and the upper-ocean structure from the moored observations are presented in sections 4 and 5. Section 6 describes the mixed layer model and the results from model runs with varying rainfall rate and wind stress. The link between mixed layer depth and SST is discussed in section 7. Section 8 discusses the hypothesized importance of the hydrological cycle to the thermodynamics of the warm pool. An appendix provides a sim-

* Contribution No. 8952 from the Woods Hole Oceanographic Institution.

Corresponding author address: Dr. Steven P. Anderson, Dept. of Physical Oceanography, Woods Hole Oceanographic Institution, Woods Hole, MA 02543-1541.
E-mail: sanderson@whoi.edu

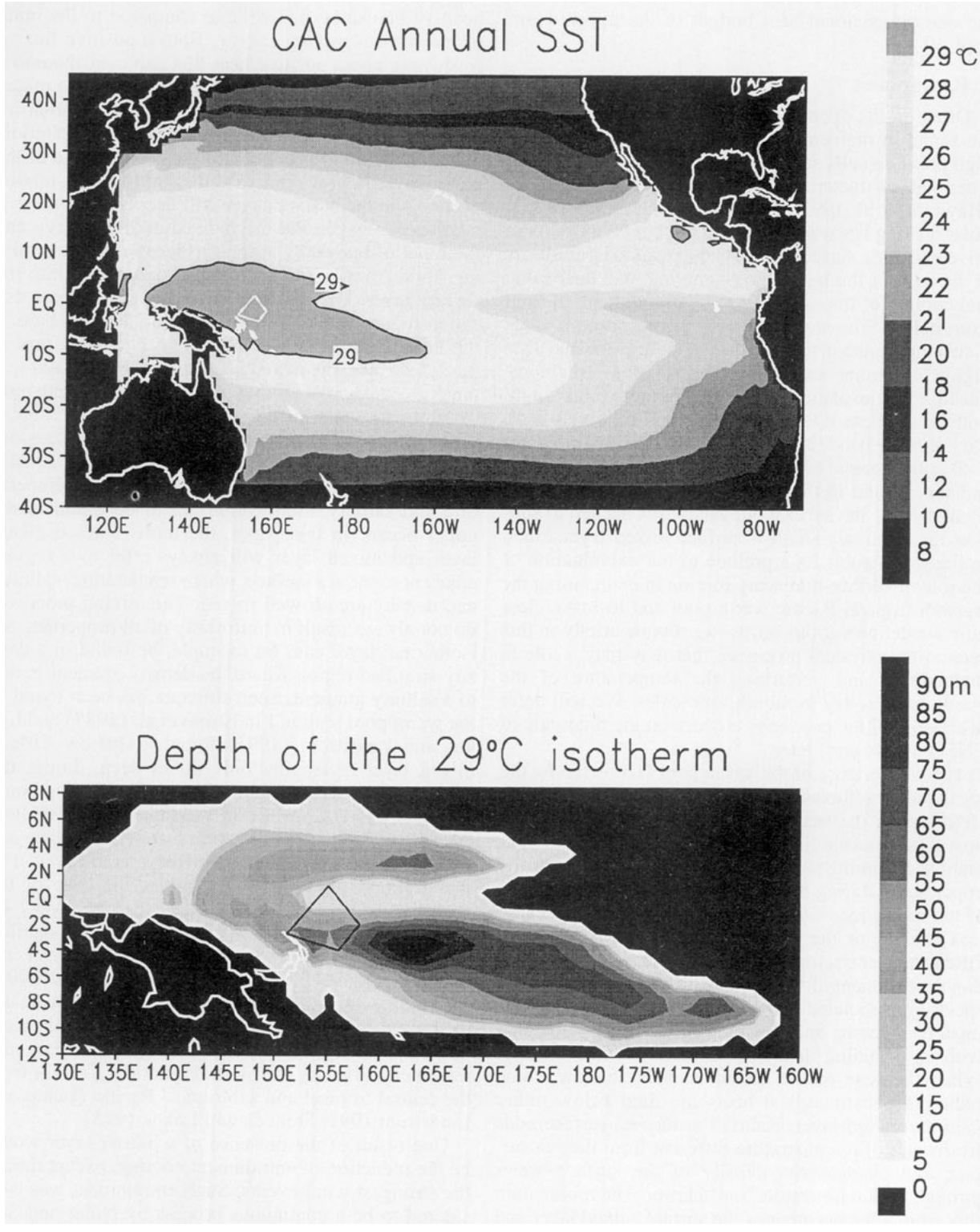

FIG. 1. Annual-mean sea surface temperature from the NOAA NMC Climate Analysis Center analyses (upper panel), with the COARE Intensive Flux Array indicated by white line segments. The western equatorial Pacific is shown in the lower panel, with contours of the depth in meters of the 29°C isotherm provided by the color bar given on the right-hand side of the figure.

ple one-dimensional heat budget of the upper warm pool.

2. Background

Often, in the open ocean, large areas of warm SSTs are found in the centers of the persistent atmospheric high pressure cells such as the Bermuda–Azores high, which are characterized by clear skies and low winds (Hawkins et al. 1993; Cornillon and Stramma 1985). Solar heating is strong there, and the light winds do not drive energetic surface currents that lead to large shears at the base of the mixed layer, mixing, and deepening and cooling of the mixed layer by entrainment of fluid from below. The western Pacific warm pool provides a striking contrast to such features. It is located in a region of strong atmospheric convection, where reduced solar insolation and strong wind events might both be anticipated to work to keep SST relatively cool. On the other hand, it is also characterized by large annual rainfall rates, which may, instead of the shortwave radiation found in the center of the Bermuda–Azores high, provide the surface buoyancy flux needed to support the relatively shallow surface mixed layer found in the warm pool. As a prelude to our examination of the role of surface buoyancy forcing in maintaining the western tropical Pacific warm pool and to make clear how we define various terms, we review briefly in this section the physical processes that may play a role in maintaining and perturbing the temperature of the warm pool on day to month timescales. We will defer discussion of the processes at work on the timescale of ENSO events until later.

The temperature of the warm pool is affected by the local air–sea fluxes of heat, mass, and momentum. Heat loss at the sea surface is associated with latent heat flux, sensible heat flux, and the net longwave radiation. Incoming shortwave penetrates and warms the upper ocean during the day, typically changing the sign of the net surface heat flux from the negative (oceanic loss) values of the night to positive during the day. Often the penetrating radiation is parameterized as a double exponential function, with the red part of the spectrum associated with an e-folding depth of approximately 1 meter and the blue–green part associated with an e-folding depth of 15 meters (Jerlov 1968). When the base of the mixed layer is shallow, some radiation penetrates and heats the fluid below rather than the mixed layer. Rainfall at the sea surface adds freshwater of a temperature different from the sea surface and changes the density of the surface water through both temperature and salinity. The momentum flux from wind accelerates the surface mixed layer and provides mechanical mixing energy. The surface buoyancy flux is the net contribution of the surface heat flux and the surface freshwater flux to changes in the surface-layer density.

Restratification and shoaling of the mixed layer occurs in light winds when the stabilizing effect from a positive buoyancy flux is large compared to the input of mechanical mixing energy. Both a positive flux of freshwater and a positive heat flux can contribute to a positive buoyancy flux and stabilize the surface mixed layer. This shoaling often occurs from strong solar insolation during daylight hours, or from precipitation. When the wind is stronger and shear at the base of the mixed layer is large relative to the stratification, mixing occurs, and the surface layer will deepen until there is a balance between the mechanical mixing energy and the input of buoyancy at the surface. During this mixing, fluid from below is entrained and mixed into the surface layer. This mixing thus provides a process that can introduce heat and salt from below into the base of the layer. When there is a negative buoyancy flux at the sea surface, the mixed layer is destabilized and will undergo convective mixing that is limited in depth only by subsurface stratification.

Because of the heavy rain in the warm pool region, positive heat and freshwater fluxes contribute equally to the surface buoyancy flux, and as a result temperature and salinity stratification are to be found in the upper ocean. In this paper, the terms surface mixed layer and mixed layer will always refer to a region, adjacent to the sea surface, where temperature, salinity, and density are all well mixed. The mixing processes do not always result in uniformity of all properties. An isothermal layer can, for example, be found in a density-stratified region where the density gradient is due to a salinity gradient. Such structure has been found in the warm pool region. Lindstrom et al. (1987) and Lukas and Lindstrom (1991) found a shallow surface mixed layer, averaging only 30 m deep, during the Western Equatorial Pacific Ocean Circulation Study (WEPOCS). The surface mixed layer had its shallow pycnocline determined by salinity stratification; the isothermal layer was deeper than the mixed layer. The salt-stratified region that determines the base of the mixed layer has been labeled the "barrier layer" by Godfrey and Lindstrom (1989) because the stability associated with that region resists mixing over the deeper isothermal layer. Sprintall and Tomczak (1992) used the Levitus (1982) historical hydrographic dataset to show the existence, in the long-term annual mean, of the barrier layer. Below the warm pool, there is saltier water carried by the South Equatorial Current from the central tropical and subtropical Pacific (Lukas and Lindstrom 1991; Shinoda and Lukas 1995).

One result of the presence of a barrier layer would be the reduction of entrainment cooling, except during the strongest wind events. Such entrainment was considered to be a continuous process by Niiler and Stevenson (1982), but these new observations suggest that entrainment might be rare in the western equatorial Pacific. After such a strong event, both temperature and salinity profiles might, as shown in Fig. 2, be well mixed down to 60–100 m. Subsequent rainfall and moderate winds create a shallow halocline and, as a

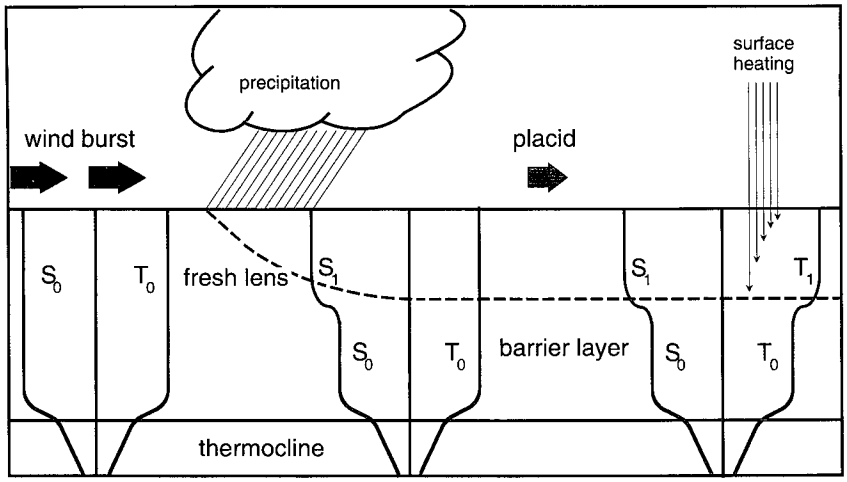

FIG. 2. Schematic diagram showing the Lukas–Lindstrom "barrier layer" theory. During a strong wind burst, the surface mixed layer extends down to the top of the thermocline. Following the wind burst, the additional buoyancy from precipitation and strong surface heating acts to form a relatively warm and fresh thin surface mixed layer. Below this thin layer is a strong halocline, which effectively decouples the surface forcing from the deeper waters. Further heating is trapped to vertical mixing above the barrier formed by the halocline.

result, a barrier layer. Later surface heating warms the surface mixed layer, and the stability of the shallow halocline limits any entrainment to be from the relatively warm barrier layer rather than from the cooler, deeper, preexistent thermocline. However, when the surface mixed layer is shallow, radiation is lost through its base.

The physical processes summarized by Fig. 2 are those that would be associated with various terms in local, one-dimensional heat and salt budgets. In addition, warm pool and upper-ocean temperatures might be affected by advection, either horizontal or vertical. Shear, and thus mixing at the base of the mixed layer, might be enhanced by flows other than the local wind-driven currents, such as the strong zonal currents found near the equator, or by internal waves. However, as a starting point, our focus is on the one-dimensional physics.

3. The experiment

As part of TOGA COARE, the Woods Hole Oceanographic Institution surface mooring was deployed in the western Pacific warm pool in the center of the Intensive Flux Array (IFA: Fig. 1) during the Intensive Observation Period (IOP: November 1992 through February 1993). The mooring was located at 1°45′S, 156°E and was deployed on 21 October 1992 and recovered on 4 March 1993. The 3-m discus buoy carried a Vector Averaging Wind Recorder (VAWR: Weller et al. 1990), which sampled wind velocity, relative humidity, air temperature, barometric pressure, incoming shortwave radiation, incoming longwave radiation, and sea surface temperature every 7.5 minutes. The time series of surface meteorological observations is continuous for 133 days except for a 4-day period, 9–13 December 1992, when the buoy was removed from the mooring to perform repairs. Several intercomparisons with both aircraft and shipboard observations validated buoy surface meteorological data. The bulk formulas of Fairall et al. (1996a,b) are used to estimate sensible and latent heat fluxes and surface wind stress. The time series of surface fluxes are shown in Fig. 3. Weller and Anderson (1996) provide a full description of the surface observations.

Precipitation data were collected on the buoy during 22 days by the Improved Meteorological Instrument (IMET: Hosom et al. 1995), which uses an R. M. Young self-siphoning gauge, which drained once full and whose volume was measured capacitively. To produce a complete time series of rainfall at the center of the IFA, observations of precipitation from the RV *Moana Wave* and the Automated Temperature Line Acquisistion System (ATLAS: Hayes et al. 1991) mooring at 2°S, 156°E were obtained. Both of these platforms employed a Scientific Technology Optical Rain Gauge (ORG). The *Moana Wave* had three cruises in the IFA during the IOP, collecting nearly 65 days of data at a location 5 km north of the WHOI mooring. Data from the buoy at 2°S were included only when both WHOI buoy and *Moana Wave* data were unavailable. There is some uncertainty as to the amplitude of the net precipitation in the IFA during COARE. Mean precipitation rates for the IFA estimated from satellite, shipboard radar, buoy and shipboard ORG, and atmospheric sounding budgets range from 5.7 to 14.0 mm day^{-1} (Bradley and Weller 1995). The resolution of differences in mean rainfall rate is

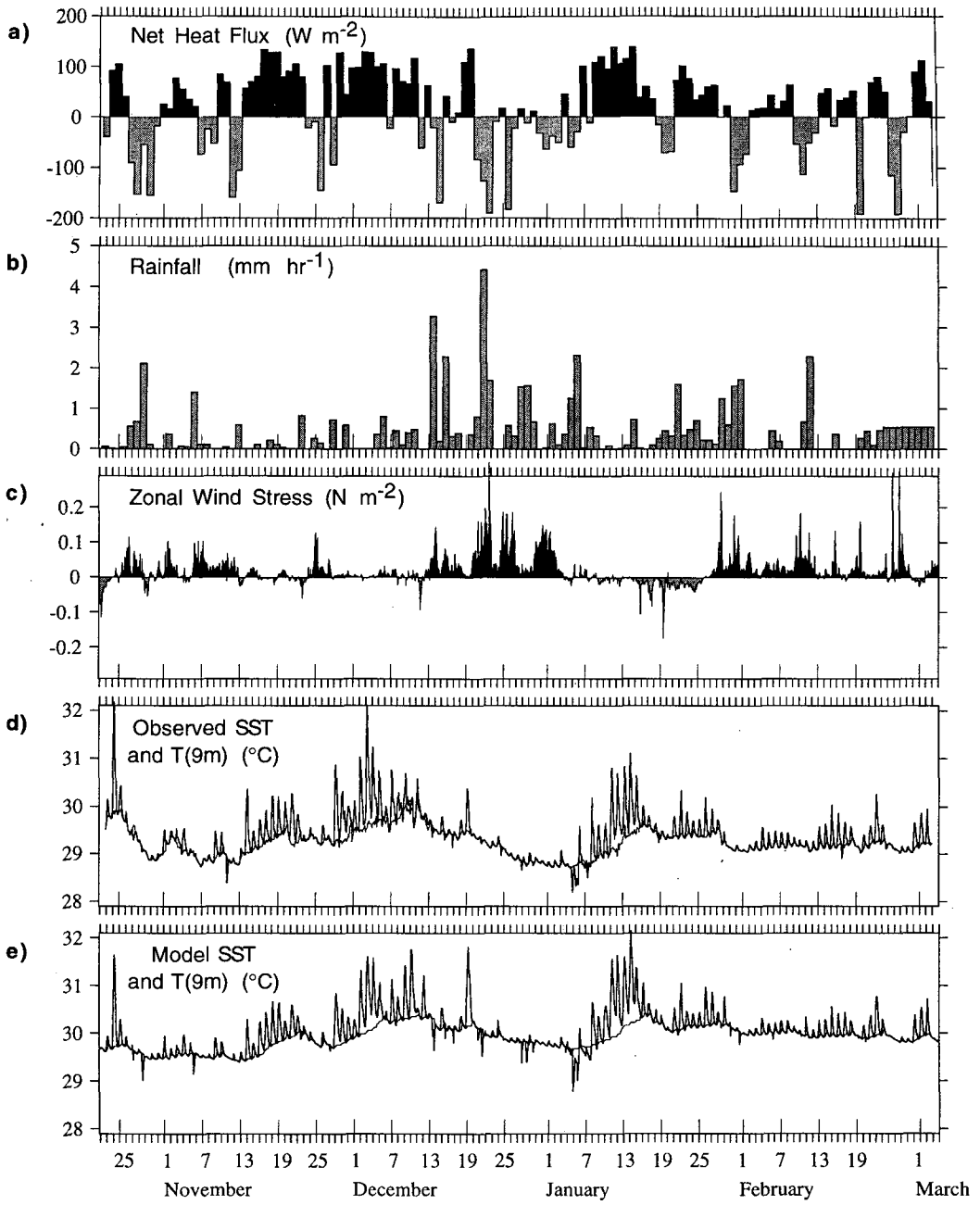

FIG. 3. Time series of the air–sea fluxes and SST from the WHOI surface mooring. Twenty-four hour averaging has been applied to the (a) net heat flux and (b) rainfall. The (c) zonal wind stress and (d) observed SST (at 0.45 m) and 9 m temperature are smoothed over 2 hours. The modeled SST (at 0.5 m) and 9 m temperature are estimated using the observed forcing and the model of Price et al. (1986). A series of three westerly wind bursts is observed in December 1992 through early January 1993.

uncertain; differences in spatial averaging, calibration techniques, and sensing systems are involved. The mean rainfall rate of the time series used in this study is 10.29 mm day^{-1}.

The mooring line was heavily instrumented in the upper 125 m of the ocean. The subsurface instrumentation consisted of 11 temperature recorders, 18 conductivity and temperature recorders (to provide salinity measurements), eight Vector Measuring Current Meters (VMCMs; to provide current and temperature), and an Acoustic Doppler Current Profiler (ADCP). Table 1 lists the instrument type and initial measurement depths

TABLE 1. Moored instrument depths. An × indicates that the instrument of the type noted was located at that depth. Here *T*, *C*, and *V* indicate, respectively, that temperature, conductivity, and velocity were measured. Instrument type is indicated by BTR for a Branker temperature recorder, SEACAT for a Seabird CTD, VMCM for a vector measuring current meter, and ADCP BIN for the depth at which the acoustic Doppler current profiler provides a velocity estimate.

Depth (m)	*T*	*C*	*V*	Instrument type	Comments
0.45	×			BTR	Sun shield
0.55	×			BTR	Sun shield
1.10	×			BTR	Sun shield
1.58	×			BTR	Sun shield
2.01	×	×		SEACAT	Buoy bridle leg
2.50	×			BTR	
4.65	×			BTR	
5.15	×		×	VMCM	
7.48	×	×		SEACAT	
8.90	×		×	VMCM	
11.52	×			BTR	
12.97	×		×	VMCM	
15.52	×	×		SEACAT	
17.01	×		×	VMCM	
19.50	×	×		SEACAT	
23.50	×	×		SEACAT	
27.50	×			BTR	
31.50	×	×		SEACAT	
39.50	×		×	VMCM	Compass malfunction after 5 Jan 95
45.50	×	×		SEACAT	
52.50	×	×	×	SEACAT, VMCM	
68.00	×	×	×	SEACAT, ADCP BIN	
76.00	×	×		SEACAT	
84.00	×	×	×	SEACAT, ADCP BIN	
92.00	×	×		SEACAT	
100.00	×	×	×	SEACAT, ADCP BIN	
108.00	×	×		SEACAT	
116.00	×		×	BTR, ADCP BIN	
124.00	×	×		SEACAT	

used in this study. The mooring line was lengthened after the surface buoy was repaired on 13 December 1992, and all the instruments below 2.5 m were shifted deeper by 2.9 m. Six temperature recorders were attached to the side of the buoy and spaced at depths from 0.45 m to 2.0 m to observe the shallow diurnal warming cycle. Predeployment and postdeployment calibrations were performed on the temperature and conductivity sensors. These calibrations, in situ comparisons with CTD casts and in line instrument intercomparisons were used to validate the measurements. Linear drifts in calibrations were removed from the near-surface temperature and conductivity records as needed. Specifically, linear drifts and biases that resulted in hydrostatically unstable profiles during times of well-mixed surface layers were removed from the top three conductivity records and temperature measurements in the top 10 m. This results in relative temperature accuracies of 0.01°C and salinity accuracies of 0.004 psu.

4. Surface buoyancy forcing

Weller and Anderson (1996) examine the surface forcing during periods of westerly wind bursts, periods of reduced convection and high solar insolation, and periods of increased convection and squalls. The convention used here is that positive buoyancy flux corresponds to the surface becoming more buoyant or lighter as a result of precipitation or heating. Periods of reduced atmospheric convection and precipitation (i.e., 30 November to 12 December 1993) have strong positive heating of the ocean and low evaporation rates due to strong solar insolation and low winds. Thus, they are characterized by strong positive buoyancy. In contrast, periods of strong atmospheric convection, such as the three consecutive westerly wind bursts (i.e., 16 December 1992 to 3 January 1993), have lower shortwave radiation and larger evaporative fluxes, which work together to remove buoyancy from the ocean surface. However, these periods also have increased precipitation, which offsets the effects of surface cooling and evaporation and can lead to net positive buoyancy fluxes.

To illustrate this effect, two-day block-averaged buoyancy fluxes are shown in Fig. 4 for the IOP. The three components of the surface buoyancy flux are calculated from the heat flux Q_{net} and from the net freshwater flux

$$B_{\text{net}} = B_{\text{heat}} + B_{\text{precip}} - B_{\text{evap}} = \alpha(C_p\rho)^{-1}Q_{\text{net}} + \beta S_0(P - E), \quad (1)$$

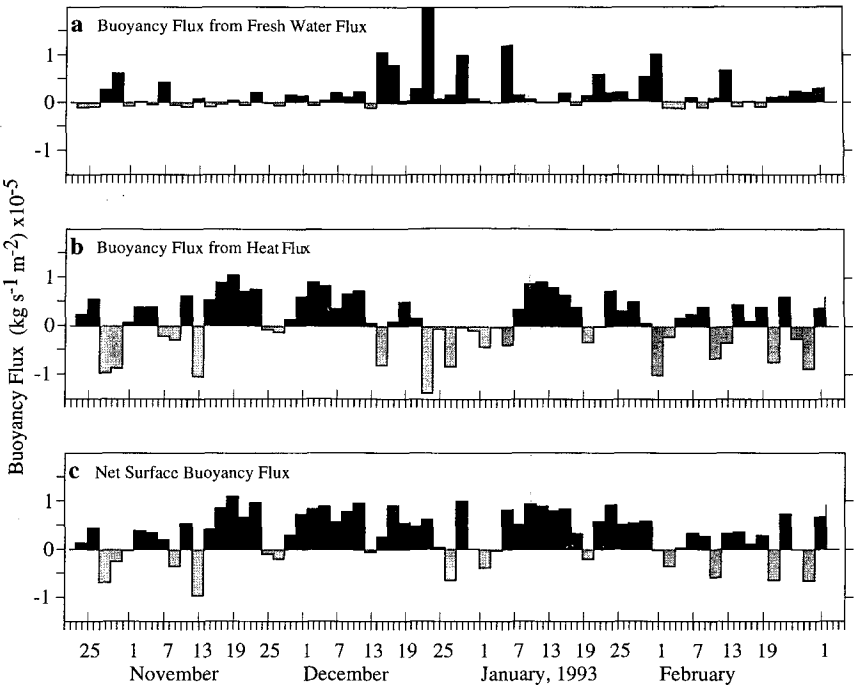

FIG. 4. Surface buoyancy fluxes. The buoyancy flux contribution from (a) the net freshwater flux ($P - E$) and (b) the surface heat flux. The net surface buoyancy flux is shown in (c). The fluxes have been block averaged over 2 days before plotting.

where α and β are the thermal and haline coefficients of expansion, S_0 is the reference surface salinity, C_p is the heat capacity, ρ is the density of sea water, P is the precipitation rate, and E is the evaporation rate. The surface heat flux component of the buoyancy flux contributes 1.15×10^{-6} kg s^{-1} m^{-2} on average over the IOP, corresponding to 14.6 W m^{-2} heating of the ocean surface. The evaporation contributes -1.11×10^{-6} kg s^{-1} m^{-2}, corresponding to 3.77 mm day^{-1}, and nearly balances the contribution from heating. The largest term is from the precipitation, which accounts for 3.01×10^{-6} kg s^{-1} m^{-2}, corresponding to 10.29 mm day^{-1}. Combining all three yields a net buoyancy flux of 3.05×10^{-6} kg s^{-1} m^{-2}. [The effects of cooling due to the rain temperature (Flament and Sawyer 1995) have been included in these calculations; this term contributes -2.9 W m^{-2} (cooling) to the net heat flux over the IOP.]

The buoyancy flux contribution from the freshwater flux (Fig. 4a) is intermittent and small except during sustained convective events. These last for up to 4 days and occur during the westerly wind bursts in late December and the squall events in late January. The heat flux contribution to the buoyancy flux (Fig. 4b) fluctuates between positive and negative. Periods of continuous positive heat flux forcing are typically longer, lasting 2 to 14 days, than periods of negative forcing, which last 2 to 4 days. The periods of negative buoyancy forcing from the heat flux often coincide with periods of positive forcing from the freshwater flux (i.e., 27–29 October 1992, 1 February 1993, 12 February 1993, and several events during mid to late December 1992.) The correlation for 2-day-averaged freshwater and heat fluxes is -0.52. The effect of the negative correlation, the surface heat flux, and the freshwater flux is to reduce the variability in the net buoyancy forcing of the ocean mixed layer on timescales longer than 2 days.

5. Mixed layer variability

The IOP mean temperature profile (Fig. 5a) is stably stratified all the way to the surface. The region of strongest temperature stratification (top of the thermocline) is located between 80 and 100 m. There is also a region of increased temperature stratification in the top 10 m of the profile. The mean salinity profile is stably stratified all the way to the surface. The region of strongest salt stratification is located at the same depth as the thermocline and little salt stratification is observed near the surface. This IOP mean profile does not exhibit a salt-stratified isothermal region above the thermocline, and there is no signature of a barrier layer existing in the IOP mean profile. However, a salt-stratified barrier layer does appear at times in the mooring record. For example, the temperature and salinity profile from 30 November 1992 reveals that below a shallow, thermally stratified mixed layer, a nearly isother-

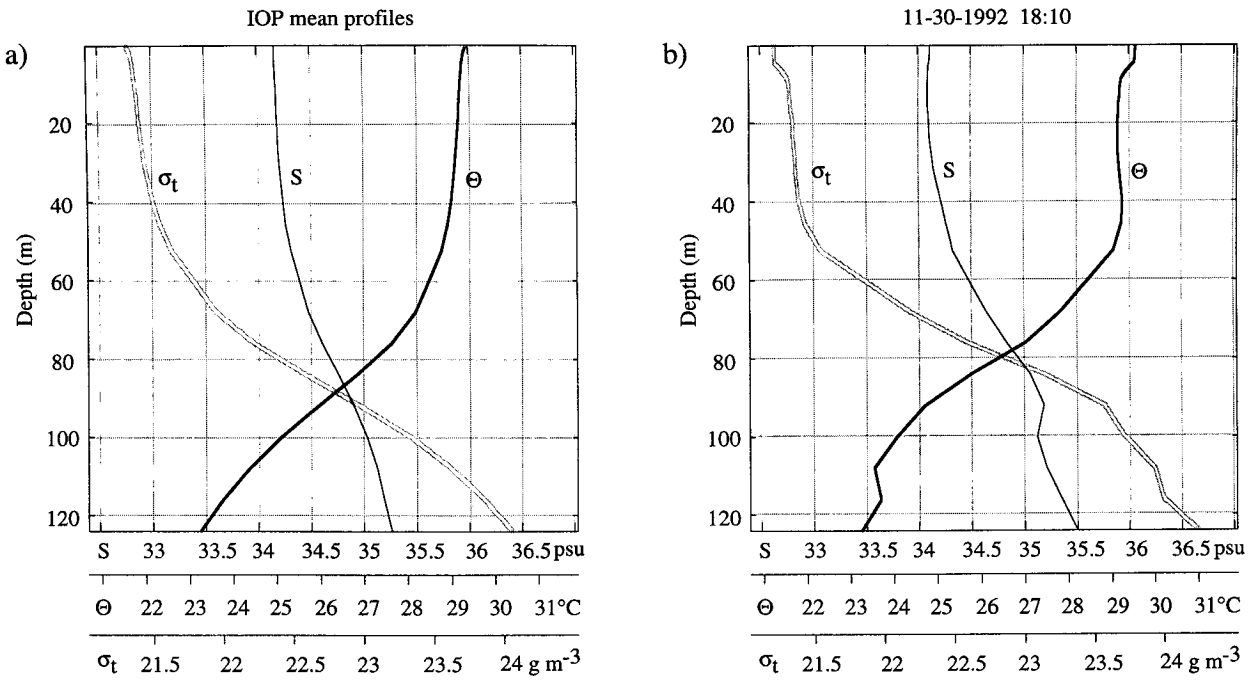

FIG. 5. Profiles of potential temperature, salinity, and potential density. (a) The IOP-mean profile reveals the top of the thermocline at 90 m, above which the temperature increases and the salinity decreases toward the surface with no clear barrier layer. (b) An individual profile taken at 1810 UTC 30 November 1992 has a shallow diurnal mixed layer above 10 m, below which the temperature is nearly constant to 50 m. This constant temperature region is salt stratified and effectively acts as a barrier between the near-surface mixed layer and the deep thermocline.

mal region exists down to 30 m and a thermal inversion layer between 30 and 50 m (Fig. 5b). This region is hydrostatically stable due to the salt stratification. A deepening surface mixed layer would need to penetrate through the salt-stratified region. The deepening would occur without entrainment cooling but, in fact, entrainment warming would take place until the mixed layer base reached depths below 50 m. This section describes the temporal variability of the observed near-surface isothermal and isohaline layers.

a. Definition of iso-layers

Recently, several criteria have been used with hydrographic data from the warm pool to define the depth of the upper-ocean isolayer, the well-mixed near-surface layer where both temperature and salinity are uniform, in the warm pool. These criteria use two methods, one based on a maximum vertical gradient and the other on the difference from the surface value. The gradient criterion assumes that there is a sharp interface at the

TABLE 2. Recent mixed layer depth criteria.

	Type of criterion	Density (H_D)	Temperature (H_T)	Salinity (H_S)
Bathen (1972)	Gradient		$\frac{\Delta\theta}{\Delta z} = 0.02°\text{C m}^{-1}$	
Lewis et al. (1990)	Difference	$\Delta\sigma_t = 0.13$ kg m^{-3}		
Levitus (1982)	Difference	$\Delta\sigma_t = 0.125$ kg m^{-3}	$\Delta\theta = 0.5°\text{C}$	
Lukas and Lindstrom (1991)	Gradient	$\frac{\Delta\sigma_t}{\Delta z} = 0.01$ kg m^{-4}	$\frac{\Delta\theta}{\Delta z} = 0.025°\text{C m}^{-1}$	$\frac{\Delta S}{\Delta z} = 0.01$ psu m^{-1}
Peters and Gregg (1987)	Difference	$\Delta\sigma_t = 0.01$ kg m^{-3}		
Sprintall and Tomczak (1992)	Difference	$\Delta\sigma_t = \alpha\Delta\theta$	$\Delta\theta = 0.5°\text{C}$	
Richards et al. (1995)	Gradient	$\frac{\Delta\sigma_t}{\Delta z} = 0.01$ kg m^{-3}	$\frac{\Delta\theta}{\Delta z} = -0.031°\text{C m}^{-1}$	$\frac{\Delta S}{\Delta z} = 0.013$ psu m^{-1}

TABLE 3. Statistics of the observed surface-layer depths in meters.

	Near-surface-layer depth			Daily maximum depths		
	H_D	H_T	H_S	H_D	H_T	H_S
	$\Delta\sigma_t > 0.01$ kg m^{-3}	$\Delta\theta < -0.03$°C	$\Delta S > 0.0133$ psu	$\Delta\sigma_t > 0.01$ kg m^{-3}	$\Delta\theta < -0.03$°C	$\Delta S > 0.0133$ psu
Mean	14.8	20.3	29.3	27.4	36.1	39.9
Minimum	0.5	0.5	2.5	2.5	2.5	3.5
Maximum	54.0	83.0	80.0	54.0	83.0	80.0
Std dev	13.4	19.4	14.9	14.1	21.3	13.9
	$\Delta\sigma_t > 0.167$ kg m^{-3}	$\Delta\theta < -0.5$°C	$\Delta S > 0.222$ psu	$\Delta\sigma_t > 0.167$ kg m^{-3}	$\Delta\theta < -0.5$°C	$\Delta S > 0.222$ psu
Mean	44.9	52.4	61.7	62.2	71.6	77.0

base of the isolayer, detectable in the first derivative, and can only be used with profiles of temperature and salinity that adequately resolve sharp gradients. The gradient criterion is attractive since the buoyancy force that turbulent kinetic energy must overcome to drive vertical mixing is directly proportional to the density gradient. The criterion, based on a difference from the surface value criterion, can be used with both vertical profile data and sparsely spaced data from moorings or climatological datasets. Several such mixed layer criteria that have been used in the warm pool region are listed in Table 2.

Our isothermal and isohaline layer depths, H_T and H_S, are defined based on a change from the surface rather than on gradients. The sea surface temperature is taken to be the temperature observed at 0.45 m. The shallowest salinity measurement is at 2 m, and salinity is assumed constant from 2.0 to 0.45 m when there is a stable temperature layer above 2 m. When there is a near-surface temperature inversion, the salinity above 2 m is estimated from the temperature profile by assuming a linear T–S relationship between the T and S at 2.0 m and freshwater at the surface with an average temperature of 22°C (the wet-bulb temperature). We recognize that this is only reasonable while it is actually raining, but do it in order to produce a hydrostatically stable density profile in the top 2 m. Here H_S is calculated by finding the minimum salinity point in the top 20 m and starting the differencing from that point downward. Likewise, H_T is calculated by finding the maximum temperature point in the top 20 m and starting the differencing from that point downward. This prevents near-surface temperature and salinity inversions from influencing H_S and H_T.

The layer depth, H_D, is calculated using a change in density from the surface. Peters and Gregg (1987) found that a density change of 0.01 kg m^{-3} demarcated the region of strongest mixing and located the base of the mixing layer through the diurnal cycle. Here we will follow the density mixed layer criterion of Peters and Gregg (1987) and choose a temperature change and salinity change to define isothermal and isohaline layers that have equal contribution to the buoyancy profile, such that

$$H_D \text{ is defined by } \Delta\sigma_t = 0.01 \text{ kg m}^{-3}$$

$$H_T \text{ is defined by } \Delta\theta = \alpha^{-1}\Delta\sigma_t = -0.030\text{°C}$$

$$H_S \text{ is defined by } \Delta S = \beta^{-1}\Delta\sigma_t = 0.0133 \text{ psu}, \quad (2)$$

where σ_t is potential density (equal to the density of water at surface pressure and in situ temperature and salinity), S is the salinity, and θ is the potential temperature. By definition, H_D is equal to or less than H_T and H_S. Time series of H_D, H_T, and H_S are calculated from the 15-minute-averaged profiles from the subsurface data. The temperature, salinity, and density profiles were linearly interpolated to a 0.5-m vertical grid prior to the calculations of isolayer depths. If the base of the iso-layer has a sharp gradient not resolved by the instrument spacing, this may lead to an instantaneous error in the depth of the isolayer equal to the size of the spacing of the observations. This, however, should not lead to a systematic error in the layer depth calculations.

The IOP-mean barrier layer thickness (BL) estimated from the IMET observations is about 5 m (H_D-H_T; Table 3). Eliminating the influence of diurnal warming on the statistics by looking at the nighttime maxima of the various layer depths, the IOP-mean BL thickness is about 9 m. Using the same layer depth criterion as Sprintall and Tomczak (1992), the layer depths are deeper, but the BL thickness is about the same. The BL at the IMET site during the COARE IOP was substantially thinner than the climatological estimates of 25 m provided by Sprintall and Tomczak (1992). The possible reasons for this are given in the discussion. The mean profiles of temperature, salinity, and density (Fig. 5a) do not show evidence of the 5–10 m thick mean BL. This is due to the large variations in the BL that occurred during the IOP relative to the mean thickness. In addition, vertical displacements of the thermohaline structure blur the mean profile.

b. Evolution of the isothermal, isohaline, and isopycnal layers

Basic statistics for the layer depths are shown in Table 3. On average H_T is 9 m shallower than H_S, and H_T has a larger standard of deviation than H_S. This additional variance is from the diurnal heating cycle, which directly affects the isothermal and isopycnal layers but not the isohaline layer. Figure 6 shows a time series of the layer depths for two 14-day periods. From 28 November through 4 December 1992, H_D and H_T are the same and range in depth from 0.5 to 18 m. There is a diurnal cycling of the layers in response to the surface heating and cooling. During this time period the isohaline layer is deeper than the isopycnal layer depth, and H_S is 10 to 25 m. Thus, the mixed layer is defined by thermal stratification rather than salt stratification. For much of the day prior to this period, the isothermal layer extended down to nearly 60 m, while the isopycnal layer was only 20 to 30 m deep, defined by the halocline. Thus, during 27–28 November there was a transition from a salt-stratified to a thermally stratified mixed layer base.

The shift from a salt-stratified to a thermally stratified mixed layer base is of particular interest during the end of the series of three consecutive westerly wind bursts, which had an average wind speed of 7 m s^{-1} and maximum winds of up to 15 m s^{-1} (Weller and Anderson 1996). This is also a time period of heavy precipitation, providing a strong freshwater flux. From 30 December 1992 to 3 January 1993 (Fig. 5), a shallow (10–20 m) thermally stratified mixed layer base is found during daylight hours and a deep (45 m) salt-stratified mixed layer base at night. The nighttime isothermal layer extends below 70 m at times. Thus, even after a series of westerly wind bursts there is a salt-stratified region, which traps the diurnal penetration of the mixed layer within the top 50 m.

The salt-stratified deep mixed layer base, with a nearly isothermal region below, observed during the westerly wind bursts matches the thermohaline structure described in the barrier-layer hypothesis. During the night, the observed isothermal layer continues to deepen 15 to 25 m below the isopycnal layer, which stays trapped at 45 m. Peters and Gregg (1987) report on observations of a diurnal cycle in the turbulence below the equatorial mixed layer. They suggest that internal waves that propagate away from the base of the mixed layer drive mixing in waters below. In addition, the surface momentum forcing is strong during this period, leading to large shears at the base of the mixed layer, which might also drive this sort of mixing. It is curious that this mixing weakens the thermal stratification but not the halocline. Note that the thermal forcing at the top of the mixed layer from air–sea fluxes and at the bottom of the mixed layer from entrainment both lead to cooling and together would weaken the thermal stratification. In contrast, the positive freshwater flux at the surface, which would support salt stratification at the mixed layer base, is opposed by the entrainment of salt at the mixed layer base. The range of values and standard deviation of H_T is larger than that of the H_D and H_S. The distribution of H_T is bimodal with a peak at the surface and at 55-m depth. This deeper peak is deeper than the maximum observed isopycnal layer depth. This bimodal isothermal layer distribution in the western equatorial Pacific was also observed by Lukas and Lindstrom (1991) using a mixed layer depth criterion based on a gradient, rather than a difference.

To examine the effects of salt stratification on low-frequency variability in mixed layer depth, we consider just the maximum depth of the mixed layer for each 24-h period. A time series of the daily maximum depth for H_D, H_T, and H_S is shown in Fig. 7, and the statistics are given in Table 3. The daily maximum H_D shoals and deepens in response to wind forcing. Shoaling to depths less than 20 m is observed during three periods: 16–21 November 1992, 27 November–7 December 1992, and 4–16 January 1993. During these low-wind periods, the surface buoyancy flux is dominated by the surface heating, a shallow H_T controls the depth of the mixed layer base, and the daily maximum H_S is typically 10 to 30 m deeper. On 12 December, the daily maximum H_D begins to deepen in response to the start of the westerly wind bursts, reaching a maximum depth of 50 m 7 days after the onset of the sustained wind forcing. The daily maximum H_D is found between 40 and 50 m until the end of the third wind burst. This period has steady wind forcing and high precipitation rates. Daily maximum H_T is consistently deeper than H_S, indicating that mixed layer deepening is limited by salt rather than thermal stratification. Daily maximum H_T deepens below 80 m reaching the top of the thermocline in late December. The components of buoyancy forcing are well correlated during February with the separate components of buoyancy flux reversing sign every 2 to 4 days (Fig. 4). At the same time, the density gradient at the mixed layer base is alternatingly thermally and salt stratified. These observations suggest that, when the surface buoyancy forcing is dominated for more than a day by positive heat fluxes, mixed layer deepening will be limited by thermal stratification and, when the surface buoyancy forcing is dominated by rainfall, mixed layer deepening will be limited by salt stratification.

6. Modeling warm pool response

a. One-dimensional mixed layer model

To illustrate the role of local precipitation in the mixed layer, we employ a one-dimensional mixed layer model (Price et al. 1986). This model assumes that salinity, temperature and current are mixed in similar ways. There is a well-mixed, homogeneous surface

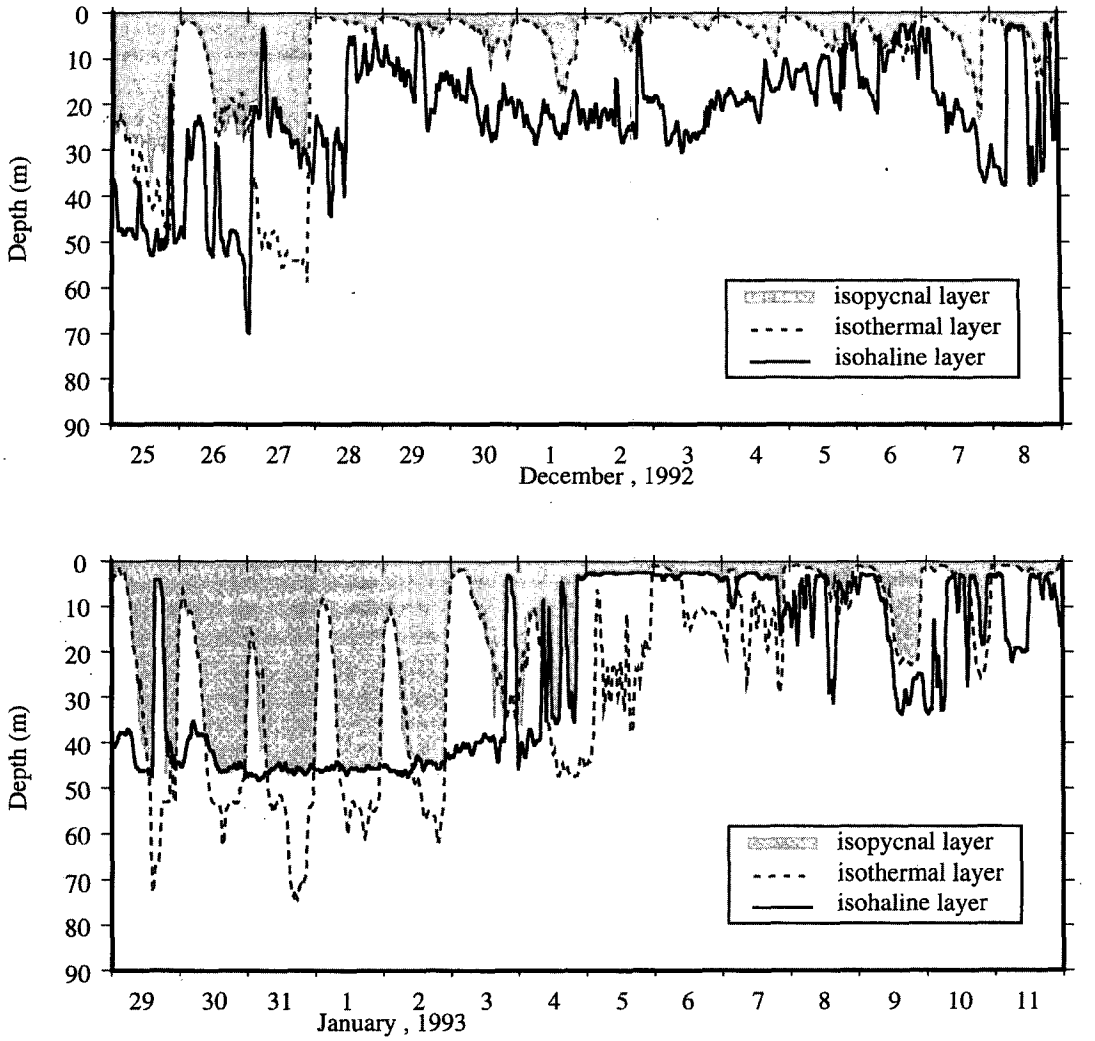

FIG. 6. Diurnal variability of the near-surface layers: H_D (gray shading), H_T (dashes), and H_S (solid line) are plotted for two 2-week time periods during the IOP to illustrate the diurnal variability in the depths. The depths are calculated from the 15-min averaged temperature and salinity records, then averaged over 1 hour prior to plotting.

layer or "slab" in which the salinity, temperature, and velocity are constant to the depth of the mixed layer base. The momentum flux, derived from the wind stress, is evenly distributed over this mixed layer. The depth of the mixed layer is determined by a stability condition on a bulk Richardson number that depends on the vertical velocity shear and the density stratification at the base of the mixed layer. When the stratification at the base of the mixed layer is too weak to support the shear, the mixed layer is presumed to deepen by turbulent mixing and thus relieve the instability. The mixed layer may also deepen if the hydrostatic stability condition is not met. In this manner, sufficient surface cooling or evaporation will drive turbulent convection and deepen the mixed layer until the hydrostatic instability is relieved. Below the mixed layer is a sheared transition layer, which simulates a region of shear flow between the base of the slab mixed layer and the fluid below. Mixing in the transition layer occurs to relieve a gradient Richardson number criterion.

When the surface buoyancy flux supplies excess buoyancy to the mixed layer, the stratification and stability at the base of the mixed layer is enhanced, thus inhibiting mixed layer deepening. The sensible and latent heat flux, the longwave radiation, and the freshwater flux are applied at the ocean surface and work to modify the buoyancy of the mixed layer. The precipitation temperature is assumed to be the same as the wet-bulb temperature (Weller and Anderson 1996). A sensible heat flux from the rain is calculated using the observed SST, rain temperature, and rain rate. This term

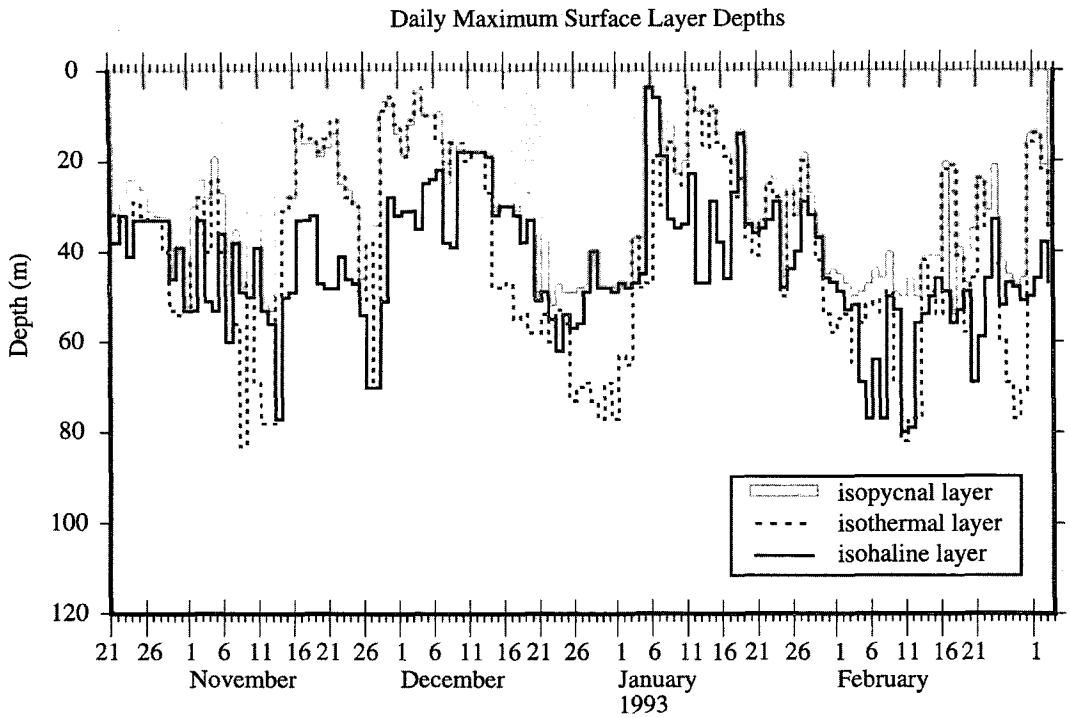

FIG. 7. Daily maximum near-surface layer depth. The maximum diurnal depth H_D (gray shading), H_T (dashes), and H_S (solid line) are plotted for the whole IOP. The isopycnal layer depth is shallower than or equal to the isothermal and isohaline depths. When the isothermal layer depth is near or equal to the isopycnal depth, the base of the mixed layer is thermally stratified. When the isohaline is near or equal to the isopycnal depth, the base of the mixed layer is salt stratified.

is added to the surface cooling terms in the model as a heat flux. The model precipitation temperature is then set to the modeled sea surface temperature. This allows the model to be forced with different rain rates without changing the net heat flux forcing. Heating from the shortwave radiation is applied as a function of depth, as prescribed by a double exponential solar extinction profile. Thermal restratification occurs when the surface waters gain heat and become more buoyant than the waters below. The bottom of the mixed layer thus shoals during the daytime. The freshwater flux from precipitation and evaporation is treated as a mass flux, and can strengthen or weaken the stratification at the base of the mixed layer by changing the salinity.

This model was modified for use on the equator by Schudlich and Price (1992) to include a prescribed upwelling, zonal pressure gradient, and equatorial undercurrent (EUC). Using this model with data from the 1984 Tropic Heat Experiment, they were able to demonstrate the skill of the model in reproducing the observed diurnal cycle of temperature, velocity, and dissipation in the surface mixed layer. They concluded that while the upwelling and zonal pressure gradient have little effect on the daytime phase of the diurnal cycle, the location and strength of the EUC did play a role in the nighttime phase of the diurnal evolution of the diurnal mixed layer depth.

The moored current observations reveal a weak EUC. The mean zonal currents have a maximum eastward flow of 28 cm s^{-1} at 275-m depth. There is weak mean shear in the upper 100 m with the near-surface current flowing toward the east at 8 cm s^{-1} and the current at 100 m flowing toward the southwest at 9 cm s^{-1}. The standard deviation of the observed currents in the top 100 m ranges from 15 to 25 cm s^{-1}, and the mean shear structure is not characteristic of individual velocity profiles. The effects of the mean shear and EUC on the mixed layer are thus assumed to be small and are left out of the model. The mean pressure gradient and upwelling are taken to be zero. One-dimensional heat budgets of the upper-ocean, determined using the mooring data, indicate a balance between the surface fluxes and local heat storage, suggesting that horizontal advection of heat is often small and that the one-dimensional model may be appropriate for most time periods. The one-dimensional salt budget, on the other hand, indicates that horizontal advection of salt is often significant. Further discussion of the success of the one-dimensional heat and salt budgets is given in the appendix.

The model is initialized with the mean temperature and salinity profiles based on the moored instrumentation, rather than the initial profile, since these are more representative of the mean thermocline, halocline,

TABLE 4. Statistics of model and observed layer depths for the duration of the IOP. Depths are in meters.

	Mean layer depth			Mean of daily maximum depths		
	H_D	H_T	H_S	H_D	H_T	H_S
			Observed			
	14.8	20.3	29.3	27.4	36.1	39.9
			Model			
$0.0 \times P_{obs}$	26.6	26.0	61.3	44.6	44.2	61.8
$0.5 \times P_{obs}$	21.5	25.2	40.6	37.7	45.3	47.4
P_{obs}	17.2	24.3	28.2	31.0	46.6	35.5
$1.5 \times P_{obs}$	14.4	24.7	22.1	26.6	48.7	29.5
$2.0 \times P_{obs}$	12.8	25.7	18.8	24.0	49.8	26.3
$2.5 \times P_{obs}$	11.7	26.9	16.3	22.2	51.7	22.9
$3.0 \times P_{obs}$	10.6	28.6	14.2	20.2	54.6	20.3

and pycnocline depths. The vertical resolution of the model is 0.25 m, and the time step is 15 min. The surface layer depths H_T, H_S, and H_D are calculated by sampling the model profiles at the observation depths and then using the algorithms described above. Next, the results from three model runs are given. In run P1, the model is driven using the observed surface forcing time series from the mooring (Weller and Anderson 1996). In run P0, the model is driven with zero precipitation and in run P2 the precipitation is set to double the observed values. Additional model runs were also done at 0.5, 1.5, 2.5, and 3.0 times the observed precipitation rate, and the results are included in the summary tables.

b. *Model results: Full buoyancy forcing*

Tables 4 and 5 summarize the IOP means and rates of change in SST for the wind bursts and subsequent restratification for the observations and these model runs. With full the buoyancy forcing (P1: Figs. 8 and 9), the mixed layer, from 25 November to 8 December, is most often defined by a shallow diurnal isothermal layer, closely following the observed diurnal variability. The model H_S approaches the surface during rain events. (Note that the timing of the rain events used to force the model may not always match those at the buoy since some of the rain observations are made from the *Moana Wave* and the ATLAS buoy.) The model H_S deepens to 45 m between rain events, while the observed isohaline layer is trapped to the top 30 m from 29 November to 6 December. Transition to a deep, salt-stratified mixed layer base from a shallow, thermally stratified mixed layer base is observed during the end of the westerly wind burst (WWB) from 29 December 1992 to 3 January 1993. The model reproduces this diurnal shifting, but the amplitude of the isothermal layer displacement is much smaller in the model than in the observations. The observed isothermal layer becomes very shallow (<15 m), while the model does not. There is a rapid rise of the model mixed layer on 4 January 1994 following the wind burst. The shallow

TABLE 5. Average rates of change in observed and model SST. Rates are in degrees Celsius per month.

	January restratification (5–15 Jan 93)	December westerly wind bursts (15 Dec 92–2 Jan 93)	IOP (21 Oct 92–4 Mar 93)
		Observed	
	4.155	−1.218	−0.179
		Model	
$0.0 \times P_{obs}$	2.516	−0.625	0.073
$0.5 \times P_{obs}$	2.917	−0.638	0.094
P_{obs}	3.475	−0.662	0.103
$1.5 \times P_{obs}$	3.849	−0.663	0.098
$2.0 \times P_{obs}$	4.325	−0.687	0.086
$2.5 \times P_{obs}$	4.125	−0.746	0.076
$3.0 \times P_{obs}$	4.222	−0.782	0.034

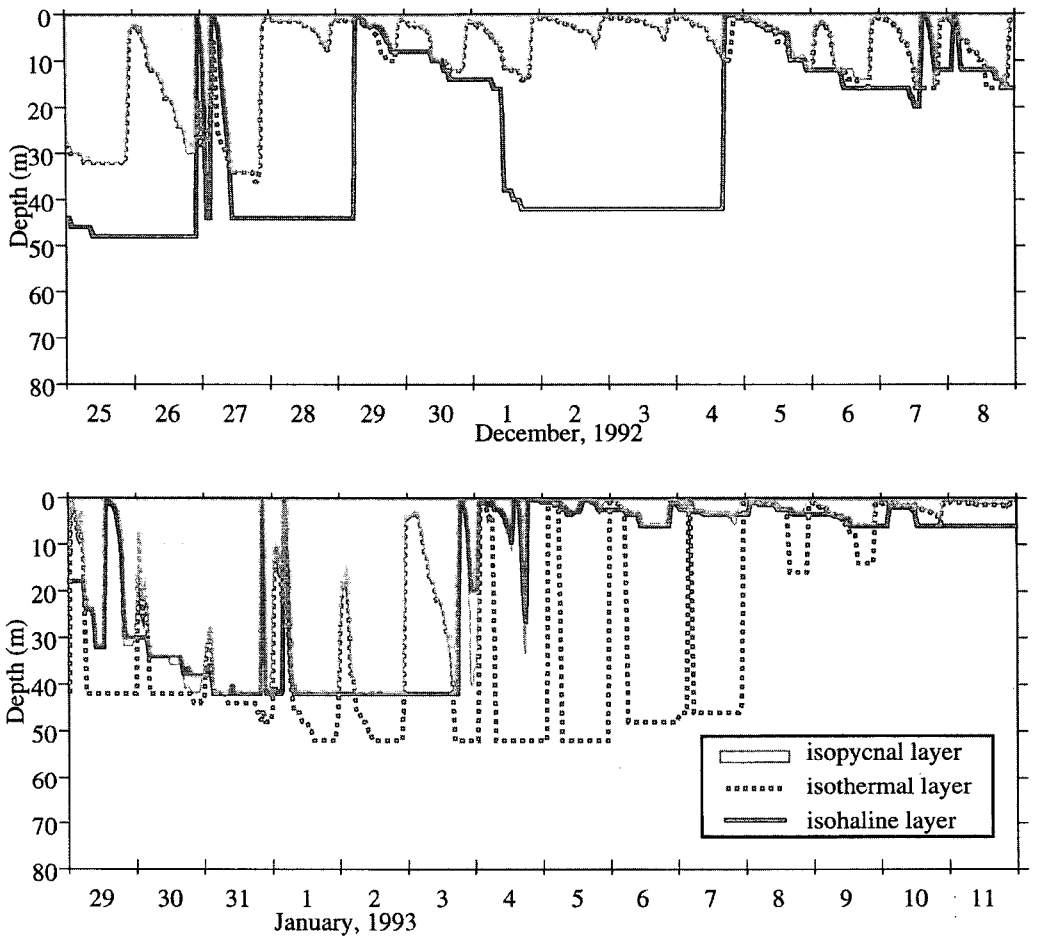

FIG. 8. One-dimensional model near-surface layers. The one-dimensional mixed layer model H_D (gray shading), H_T (dashes), and H_S (solid line) are plotted for the same 2-week time periods as shown in Fig. 4. The full surface forcing has been used in run P1.

mixed layer has a salt-stratified base and does not deepen below 10 m until after 11 January 1993. The isothermal layer continues to rise until it supports a shallow diurnal mixed layer on 10 January 1993.

The daily maximum model layer depths are shown in Fig. 9. The observed layer depths (Fig. 7) have much more day to day variability than the model depths, but there is good agreement between the model and observed depths on longer time scales. The model shoals during the low wind events and deepens during the higher wind events. Even though there is a positive net buoyancy flux, the model mixed layer depth does not continue to shoal during the IOP. The statistics of the model layer depths (Table 4) are nearly consistent with those of the observations. The one striking difference between the model and observations is the high temporal variability in the observed mixed layer depth. This may have to do with the internal tide lifting the mixed layer base and the pycnocline or horizontal advection.

The model SST successfully reproduces much of the observed SST variability, and the amplitudes of the daily cycles are well matched (Figs. 3 and 10). The model SST deviates from the observed at the same times that the 1D heat budget does not close (late October, early November, westerly wind bursts; see appendix).

A shortcoming of the one-dimensional model is seen during westerly wind bursts. The isopycnal and isohaline layers, during this period, continue to deepen in the model, while the observed isohaline layer is constant at around 45 m. This suggests that there might be a persistent salt barrier that may be supported by the same advective forcings that are needed to balance the mean surface freshwater flux and maintain a near-constant layer salinity. The response of the upper equatorial ocean to large-scale westerly wind forcing is complicated by the setup of the Yoshida jet, Ekman convergence, and the generation of various equatorial waves in response to these wind bursts (Eriksen 1993;

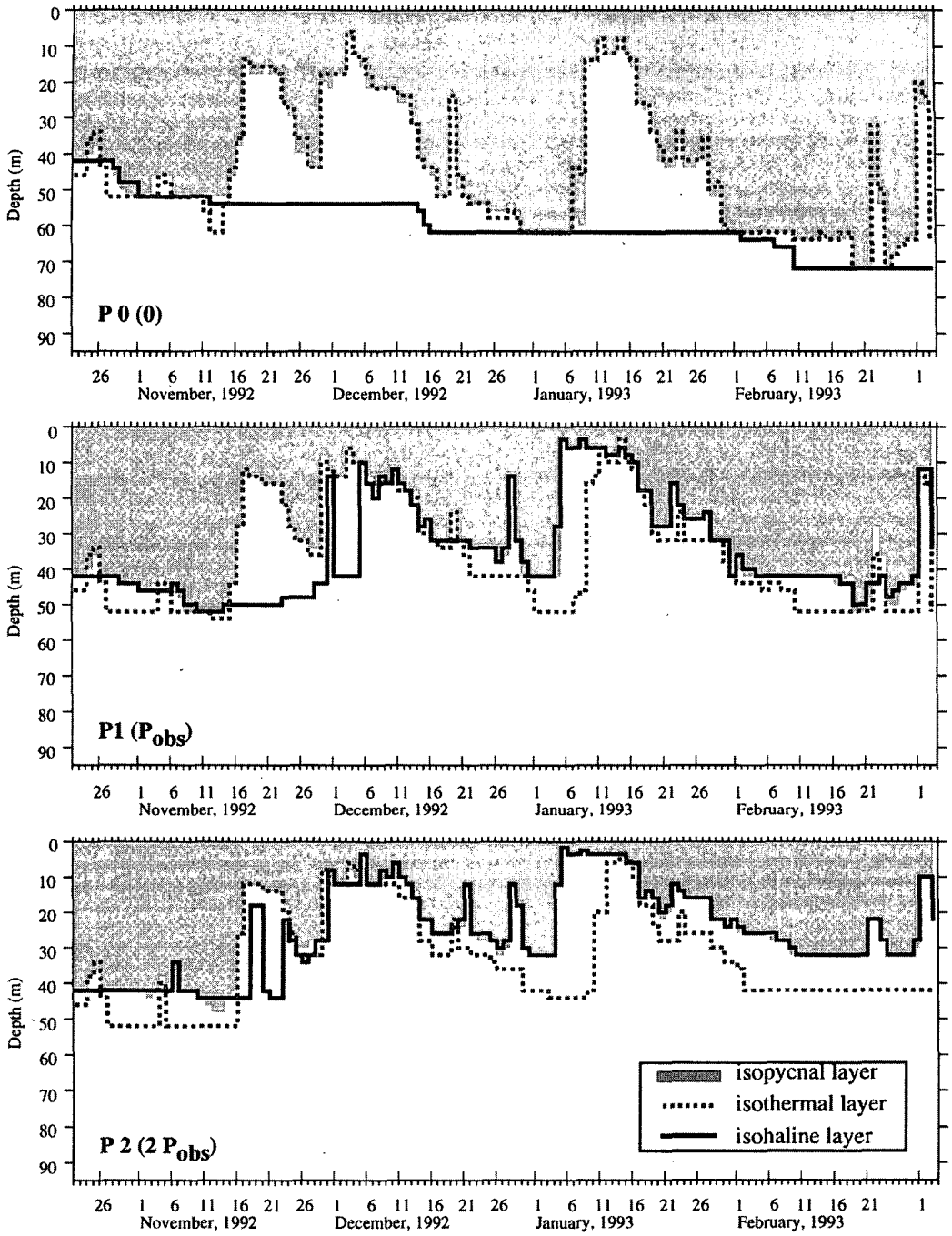

FIG. 9. Model maximum diurnal layer depths. The maximum diurnal depth H_D (gray shading), H_T (dashes), and H_S (solid line) are plotted for the same period shown in Fig. 4. The isopycnal layer depth is always shallower than or equal to the isothermal and isohaline layer depths. Shown are the results from runs (a) P0 ($P = 0$), (b) P1 (P_{obs}), and (c) P2 ($2 \times P_{obs}$). (d) Also shown are the model results from using the observed precipitation, but increasing the wind stress by a factor of 4.

Sprintall and McPhaden 1994). During late December and early January, the observed SST decreases by 1°C while the model SST decreases by only 0.3°C, and the observed sea surface salinity increases by 0.15 psu while the model decreases by 0.1 psu (Fig. 11). Also, the 1D heat and salt budgets have the largest residuals

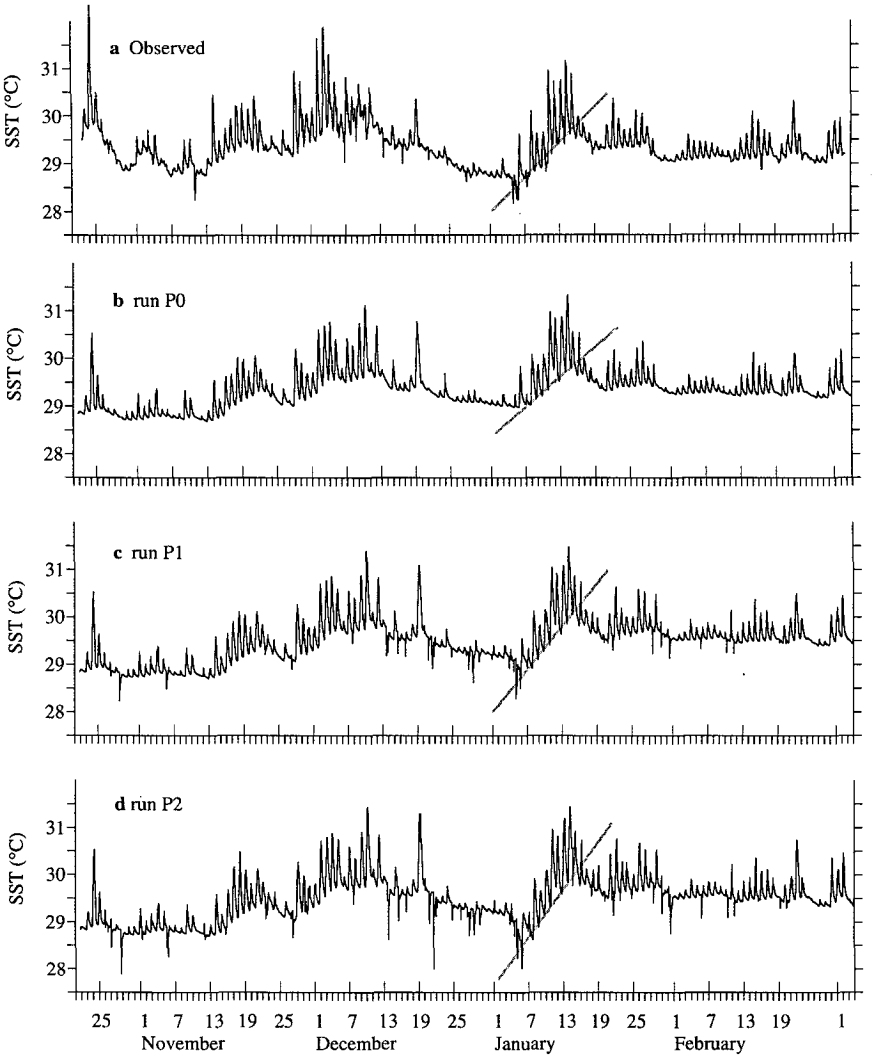

FIG. 10. Model and observed SST. The observed (a) and model SST, corresponding to runs (b) P0 ($P = 0$), (c) P1 (P_{obs}), and (d) P2 ($2 \times P_{obs}$), are plotted for the IOP. The light gray line indicates the slope of SST during the low wind period following the wind burst.

during this time. Studies that consider the three-dimensional response of the upper ocean are needed to further explore the mechanisms of entrainment of cool, salty water into the mixed layer.

c. *Model results: No precipitation*

Run P0 was conducted with precipitation set to zero. This leads to a negative freshwater flux out of the model ocean, which increases the surface salinity and, leads, overall to near-zero net surface buoyancy flux. The result is a mixed layer base that is thermally stratified and deepens over the run (Figs. 9 and 12). The diurnal variability is shown in Fig. 12 for comparison with the first model run and the observations. Following the westerly wind bursts, the restratification and shoaling of the mixed layer is delayed by 4 days, and it is not until 8 January 1993 that the mixed layer shoals above 20 m. The model mixed layer without precipitation is deeper than P1 during the low wind forcing found at the end of November and the beginning of January. The response to the WWB is a mixed layer 10 to 20 m deeper than the observations and P1. Notably absent from from run P0 are the low SST spikes found in both observations and run P1. These near-surface temperature inversions are the direct result of nighttime surface cooling acting on a shallow fresh pool of water at the ocean surface.

d. *Model results: Double precipitation*

Run P2 showed a net shoaling of the mixed layer over the 4-month period (Fig. 9). Starting in the be-

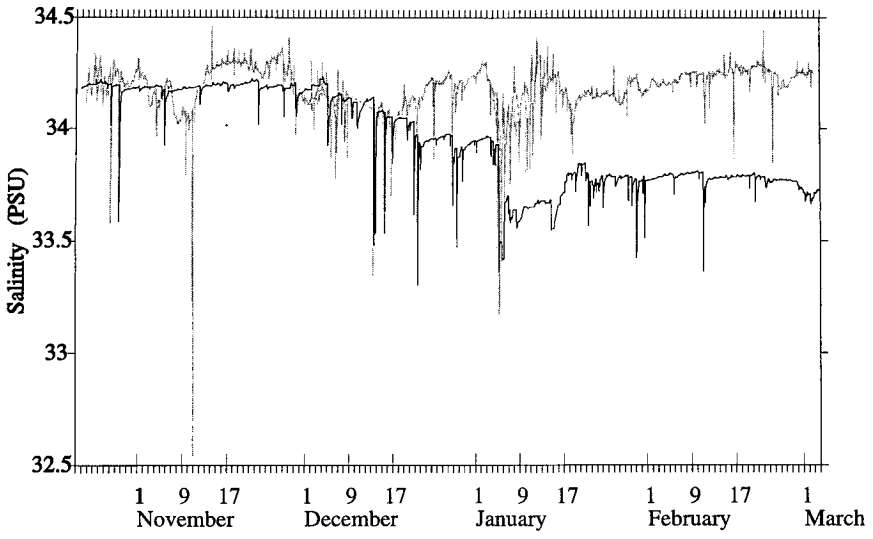

FIG. 11. Model and observed SSS. The observed (gray line) and model salinity (black line) at 2 m are plotted for the IOP.

ginning of December, the mixed layer base is solely salt stratified. Unlike the other two model runs, H_D does not continually deepen during the westerly wind bursts, while H_T does deepen. The final H_D at the end of February is 35 m, half the depth of the isopycnal layer from run P0; H_D is shallower during the low wind periods than in either of the previous runs.

e. *Wind and buoyancy forcing, and the scaling of the model mixed layer depth*

The buoyancy forcing on the mixed layer in the warm pool is positive and varies little in magnitude due to the phasing of the precipitation and wind events. Niiler and Kraus (1977) offer an equilibrium mixed layer depth scaling for times when there is increasing stability in the upper ocean and some wind forcing but insufficient to produce significant entrainment mixing. This is the depth where there is just sufficient mechanical mixing energy from the wind forcing to mix the buoyant surface water uniformly down from the surface. The equilibrium mixed layer depth, h, is

$$h \propto \frac{u_*^3}{\kappa_0 B_0} = L_b, \tag{3}$$

where h is the mixed layer depth; u_* is the surface friction velocity; B_0 is the surface buoyancy flux; L_b is the Monin–Obukhov length scale; and κ_0 is a proportionality factor, the von Kármán constant, equal to 0.42. The IOP mean wind stress ($\tau = 0.0395$ N m^{-2}) and net surface buoyancy flux ($B = 3.29 \times 10^{-8}$ m^2 s^{-3}) yield an equilibrium mixed layer depth of 17.4 m. This mixed layer depth scale is consistent with the mean mixed layer depth of model run P1.

It is not obvious that the IOP averaged PWP mixed layer depth scales with the equilibrium mixed layer depth calculated from the IOP-averaged momentum and buoyancy fluxes. The PWP model, similar to earlier bulk mixed layer models, employs a homogeneous "slab" mixed layer of a depth that is defined by a bulk Richardson number (Ri) criteria. The turbulent erosion model (TEM; i.e., Kraus and Turner 1967) uses a bulk Ri with a velocity scaling based on the wind stress friction velocity. In the TEM, under positive buoyancy forcing and wind forcing, the slab thickness is explicity equivalent to the Monin–Obukhov length derived from the surface momentum and buoyancy fluxes. The response of the TEM under positive buoyancy forcing to a step function in wind speed is simply a step function in mixed layer depth. The dynamic instability model (DIM), like the PWP model, uses a bulk Ri with a velocity scaling based on the magnitude of the velocity difference across the base of the mixed layer. The velocity in the slab layer responds to both inertial forces and wind stress. In the DIM, under positive buoyancy forcing, the slab layer velocity is first accelerated by a step function in wind forcing, and then deepening occurs when the bulk Ri becomes unstable. Price et al. (1978) show that the DIM captured mixed layer variability on diurnal and inertial timesscales better than the TEM in varied environmental conditions. An alternate to the bulk model is the turbulent-closure-type model, such as that of Mellor and Yamada (1982). In comparison of mixed layer models for the tropical ocean, Chen et al. (1994) did not report the results of the PWP model because they claim that the PWP results are nearly the same as the MY model. This is confirmed by Zhang (1995), who used the buoy flux observations from COARE in both the KT, MY, and

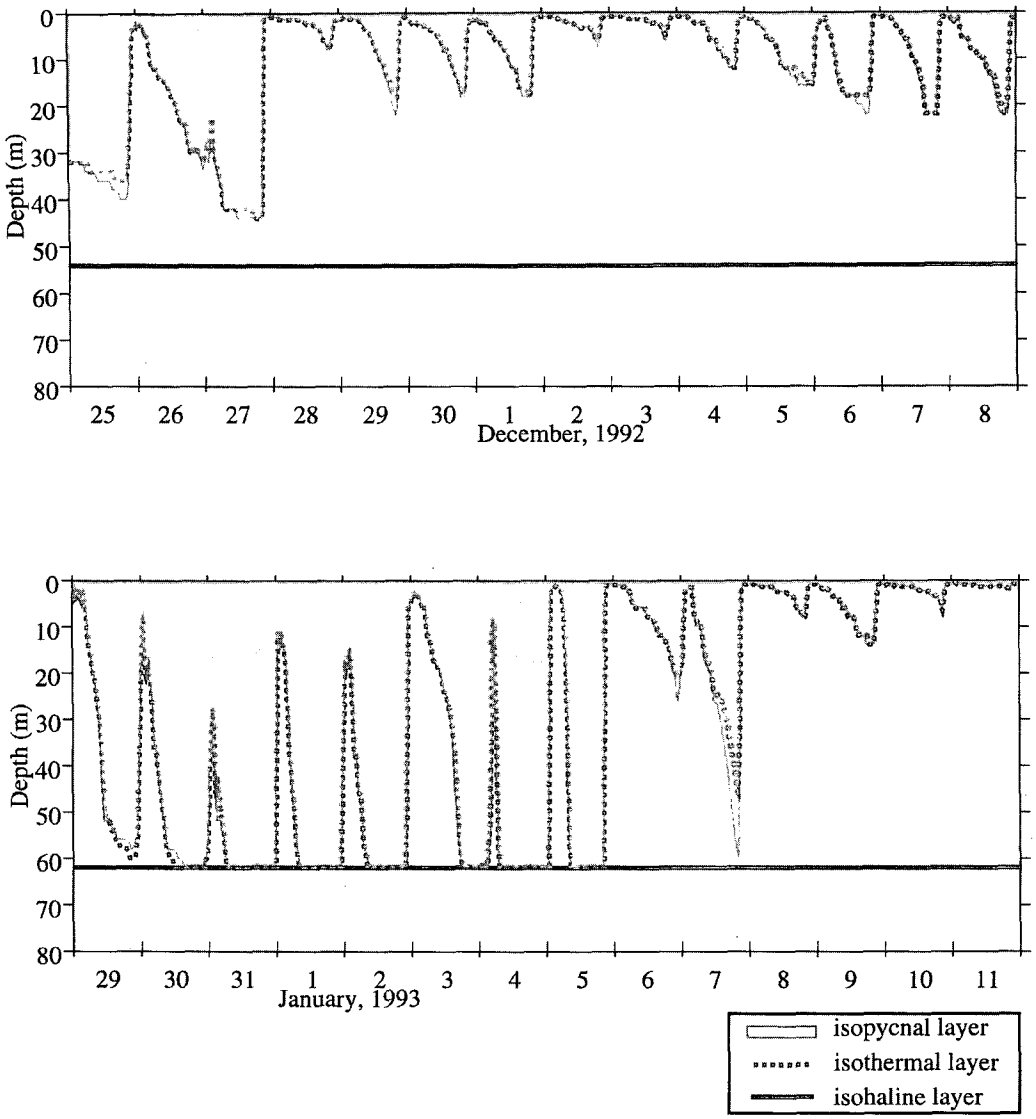

FIG. 12. One-dimensional model run with zero precipitation. The one-dimensional mixed layer model H_D (gray shading), H_T (dashes), and H_S (solid line) for run P0 ($P = 0$) are plotted for the same 2-week time periods as shown in Fig. 4. The same surface forcing is used in this run except that the precipitation rate is set to zero.

PWP models and found little difference in the MY and PWP model results. However, it is not clearly evident that the Monin–Obukhov scaling is consistent with the DIM-type PWP model. This scaling would allow the link to be clearly made between mean forcing conditions and the mean PWP model mixed layer depth.

If the Monin–Obukhov scaling holds, then the same mean model mixed layer depth could be obtained by increasing or decreasing both wind stress and precipitation at the same time. In a total of 64 model runs, the parameter space of wind and rain forcing on the model was investigated. The rain was varied from zero to three times the observations, while the wind stress was varied from zero to four times the observations (Table 6). The mean of the maximum daily mixed layer depths is plotted against the Monin–Obukhov length scale estimated from the mean forcing (Fig. 13a). Although the model mixed layer depths do not fall on the one to one line with the Monin–Obukhov length scale, the scaling does effectively collapse the model results. There is a region between $L_b = 5$ m and $L_b = 30$ m where the relationship is nearly linear. This is the region best represented by the assumed case in which there is increasing stability and some wind forcing but insignificant entrainment. For the cases in which L_b is less than 5, the effects of wind forcing are limited and the mixed layer depth is largely governed by nighttime

TABLE 6. Mean model mixed layer depths for different rain rates and wind stresses. Depths are in meters.

Wind stress ($n\tau$) n	Rain rate						
	$0.0 \times P_{obs}$	$0.5 \times P_{obs}$	$1.0 \times P_{obs}$	$1.5 \times P_{obs}$	$2.0 \times P_{obs}$	$2.5 \times P_{obs}$	$3.0 \times P_{obs}$
0.0	17.2	10.3	5.9	3.8	2.7	1.9	1.5
0.5	21.8	15.7	11.9	9.7	8.3	7.2	6.4
1.0	26.6	21.5	17.2	14.4	12.8	11.7	10.6
1.5	31.2	26.3	22.0	18.9	16.9	15.3	13.9
2.0	35.3	30.4	26.4	23.2	20.8	19.0	17.3
2.5	38.6	34.4	29.8	26.6	24.5	22.4	20.6
3.0	41.7	37.4	33.1	29.9	27.4	25.9	23.9
3.5	45.3	40.5	35.9	32.8	30.4	28.6	26.6
4.0	48.1	43.3	38.9	35.6	32.9	31.1	29.1

convection. When L_b is greater than 30 m, the entrainment and existing subsurface stratification can no longer be ignored in determining the mixed layer depth.

Monin–Obukov mixed layer scaling assumes limited entrainment. To test that the model mixed layer depth is decoupled from the thermocline depth, another set of model runs was conducted that was initialized with a two-layer temperature and salinity profile. The temperature and salinity were taken as 29°C and 34.6 psu above 150 m and 23°C and 35.6 psu below. Again, the mean model mixed layer depth is plotted against L_b (Fig. 13b). For L_b less than 50 m, the deep thermocline model runs yield mean mixed layer depths that are only slightly deeper for the same surface forcing than the previous results. The sea surface temperatures from P1 are nearly the same after the first 7 days as that from the same forcing but a deep thermocline.

7. Implications of model results

a. *Mixed layer depth and SST*

The dependence of model mixed layer depth on wind stress and precipitation found in Table 6 is such that either decreasing wind stress or increasing precipitation results in a shallower mixed layer. The net change of SST for the same set of model runs is given in Table 7. The net effect of changing wind stress and rain rate is not intuitive. For higher wind stresses, increasing precipitation increases the rate of SST warming; however, increasing precipitation rates at low wind stress leads to a decrease in the rate of SST warming. Note that the changes in SST warming are only affected by changes in wind stress and rain rate since the heat flux forcing is the same for the whole set of runs. This raises the question, What effect does the local precipitation, through its role in determining mixed layer depth, have on the SST?

There are three ways that the mixed layer depth may affect the surface temperature for the same surface heat flux: 1) Changing the mixed layer depth effectively changes its heat capacity, thus for the same surface heat flux, a shallow mixed layer will generally change temperature more rapidly than a deep one. 2) The shortwave extinction is also a function of depth and some radiation passes through the bottom of the mixed layer; thus, the radiative heating of the mixed layer is reduced as a mixed layer shoals. 3) A deepening mixed layer will eventually entrain cool water from the thermocline, effectively cooling the surface temperature.

First, we consider the case in which there is no entrainment. Combining the first two effects, the time rate of change in mixed layer temperature for a given mixing depth, h, over which heat from the surface fluxes is well mixed, is given by

$$\dot{T} = \frac{1}{\rho C_p h}\left[Q_{\text{surf}} + Q_{\text{sw}}(1 - f(h))\right], \qquad (4)$$

where $f(h)$ is the shortwave transmission at depth h; and Q_{surf} is the sum of the net longwave, latent, and sensible heat fluxes, which are applied to the ocean surface. The mixed layer will only warm if the net surface heat flux ($Q_{\text{surf}} + Q_{\text{sw}}$) is positive and the shortwave radiation transmitted out of the base of the mixed layer is smaller than the net surface heat flux. Thus, there is some crossover depth where $\dot{T} = 0$, above which there is cooling even with a positive net surface heat flux. Nearly 60% of the shortwave absorption occurs in the first few meters, so for cases with strong net heating, such as at midday, this depth may be less than a meter. [Note that this crossover occurs at the same depth as the temperature compensation depth explored by Woods (1980). In the Woods derivations, in which freshwater fluxes are neglected, the temperature compensation depth is the penetration depth of convective mixing if it is found above an existing pycnocline. The temperature compensation depth is not representative of the mixed layer in the warm pool since vertical mixing is governed by wind mixing, rather than convection, because of the strong surface buoyancy forcing from rain.]

As an example, consider the low wind period from 5 to 15 January examined by Weller and Anderson (1996) for which $Q_{\text{surf}} = -120$ W m^{-2} and $Q_{\text{sw}} = 202$ W m^{-2}. The red-light transmission profile is not well

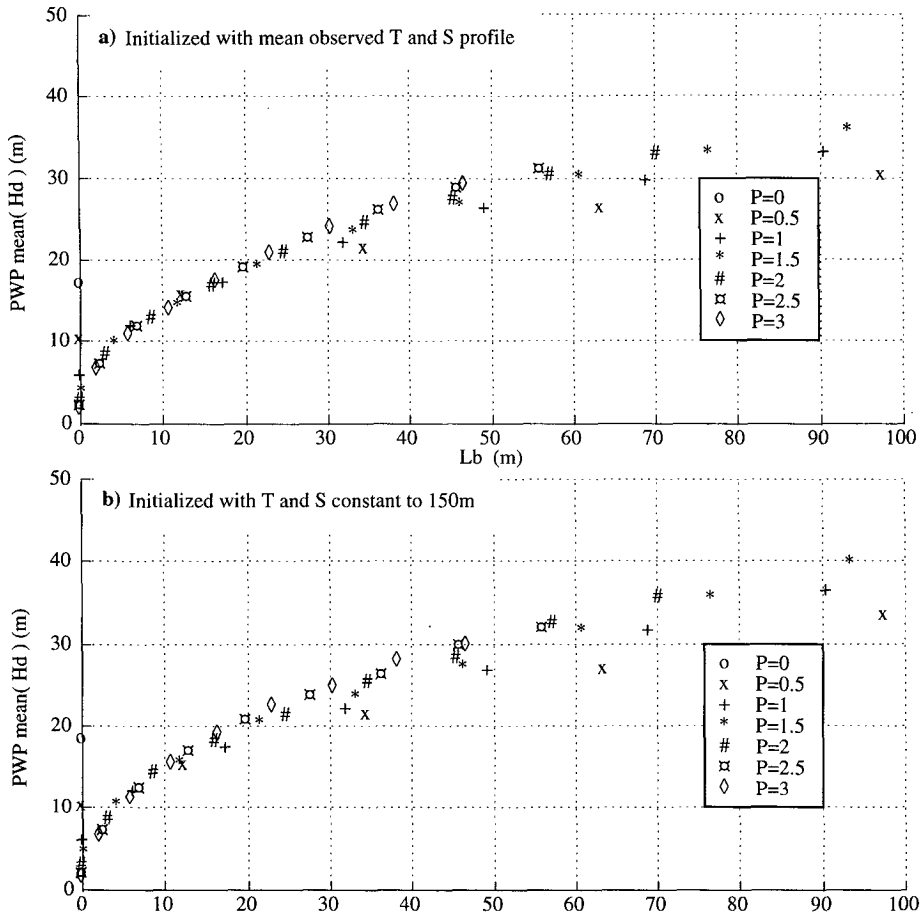

FIG. 13. Monin–Obukov scaling of PWP model mixed layer depths. The Monin–Obukov scale is calculated from the mean buoyancy and momentum forcing applied to each of 64 model runs in which the rain was varied from zero to three times the observed and wind stress was varied from zero to four times the observed values. This is plotted against the mean isopycnal mixed-layer depth for the run. For each symbol indicating P, there are six corresponding wind stresses values. (a) The model was initialized with the observed mean temperature and salinity profile (Fig. 5a). (b) The model was initialized with a constant temperature and salinity above 150 m.

know for this region, so we will use the profile for water "type 1A," given by Jerlov (1968), and plot $\dot{T}$ as a function of h (Fig. 14a). The maximum rate of layer temperature change is 2.8°C mo^{-1}, found at 3 m. For deeper mixed layers, much of the shortwave has been absorbed and $\dot{T}$ remains positive but decreases with depth since the same heat is being applied to a larger volume of water. For shallower layers, the rate becomes negative due the transmittance of shortwave through the base of the mixed layer. Thus, there is a mixed layer depth at which heating SST is maximized. The heating crossover depth occurs at less than 1.0 m. The surface layer temperature will increase as long as there mixing below the crossover and will increase the fastest if the mixed layer is only 3 m deep. If mixing penetrates deeper, the layer will still warm, but not as rapidly.

There is a rapid recovery of the SST during this low wind period that follows the westerly wind bursts. From 4 to 14 January 1993, a net change of 1.4°C at a rate of 4.2°C mo^{-1} (Table 5) and mixed layer depths ranging from 5 to 20 m was observed. The heating rates estimated from (4) for this period suggest that the rate of change in SST is sensitive to the mixed layer depth. The SST changes for this low wind period from all 64 model runs were plotted against mean mixed layer depth (Fig. 14a). Overplotted is the heating rate plotted against $0.5h$, which is a proxy for mean mixed layer depth since h represents a maximum penetration depth. Below 2 m, a shallower mixed layer leads to a more rapid rise in SST. The P1 SST underestimates the observed SST increase, with mixed-layer depths ranging from 5 to 10 m. The P0 has an even smaller SST rise with a rate of 2.5°C mo^{-1} (Table 5). This is due to the deeper mixed layer that develops when no precipitation is added to the model. For P2, the precipitation was increased by a factor of 2 over the observed values, and

TABLE 7. Rate of net changes in model SST for different rain rates and wind stresses. Rates are n°C mo.$^{-1}$

Wind stress ($n\tau$)	Rain rate						
n	0.0 × P_{obs}	0.5 × P_{obs}	1.0 × P_{obs}	1.5 × P_{obs}	2.0 × P_{obs}	2.5 × P_{obs}	3.0 × P_{obs}
0.0	0.117	0.106	−0.066	−0.845	−4.511	−4.863	−5.17
0.5	0.097	0.109	0.082	0.019	−0.071	−0.152	−0.273
1.0	0.073	0.094	0.103	0.098	0.086	0.076	0.034
1.5	0.049	0.072	0.089	0.100	0.105	0.109	0.093
2.0	0.024	0.048	0.066	0.083	0.094	0.106	0.097
2.5	−0.002	0.018	0.042	0.061	0.073	0.088	0.096
3.0	−0.027	−0.008	0.017	0.035	0.054	0.065	0.075
3.5	−0.063	−0.036	−0.009	0.010	0.028	0.039	0.054
4.0	−0.091	−0.062	−0.037	−0.019	−0.001	0.013	0.032

the resulting mixed layer depths are shallower than in P1. This leads to a larger SST increase at a rate of 4.3°C mo^{-1}, with the same heat flux.

Generally, the additional buoyancy from the precipitation inhibits mixed layer deepening, traps the surface heating to a shallower layer, and accelerates the rise in SST following the westerly wind burst. Alternately, reducing the wind forcing also leads to a shallower mixed layer and an accererated rise in SST. The model runs have higher heating rates than predicted by the simple heating rate equation. This may be due to the limitations of ignoring strong near-surface diurnal cycling and using mean heat fluxes to predict surface heating rates. Run P1 heating rates for this time period underestimate the observed changes. Siegel et al. (1995) report a phytoplankton bloom in the COARE IFA beginning on 4 January that leads to the absorption of more shortwave radiation at shallower depths, which would lead to a shallower mixed layer and more rapid warming of SST.

The effective mixed layer depth can also play a role in governing SST change during sustained cooling, as observed during the westerly wind burst period 20 December 1992 through 4 January 1992 when the mean heat fluxes were Q_{surf} = −205 W m^{-2} and Q_{sw} = 156 W m^{-2}. Again, the cooling rates as a function of mixing depth from (4) are plotted along with the change in model SST as a function of mean daily maximum mixed layer depth for all 64 model runs (Fig. 14b). The largest cooling rates are associated with the shallowest mixed layer depths, which are cases of excessive precipitation and reduced wind stress. There is a large depth range where the layer cooling is nearly constant at −0.65°C mo^{-1}. The very deepest mixed layers have slightly larger cooling rates, indicating entrainment cooling. These are the model runs with little or no precipitation and extreme wind forcing. None of the model runs fully reproduce the observed rapid decrease in SST during the westerly wind burst. The net change in SST in run P1 during the westerly wind burst is only about half the observed change. This may reflect the imbalance in the one-dimensional heat budget (see appendix) and simplicity of the model.

What is the net effect of the precipitation on SST over the 4-month IOP? The net change in SST over the whole deployment is −0.78°C. Run P1 has a mean heating rate of 0.103°C mo^{-1}; P0 has a smaller SST change (0.073°C mo^{-1}), and the mean mixed layer depth is 10 m deeper than in P1. In P2, the mean mixed layer depth is 5 m shallower than in P1, and the net change in SST is 0.086°C mo^{-1} for the same positive heat flux. Thus, both increasing and decreasing the rain rate from that observed reduces the mean SST heating rate over the 4-month period. This result demonstrates the important role of penetrating shortwave radiation, as well as entrainment.

The model of layer temperature change (4) can be used to illustrate the consequences of shortwave penetration by comparing the mixing depth h to the daily maximum layer depths since it is to this depth that the surface heat flux is mixed over a diurnal cycle. The heating crossover depth can be much deeper when there is a close balance between the shortwave heating and surface cooling terms. The time rate of layer temperature change is plotted versus mixing depth using the IOP mean heat fluxes Q_{surf} = −179 W m^{-2} and Q_{sw} = 193 W m^{-2} in Fig. 15a. The point of most rapid increase in mixed-layer temperature is at 29-m depth, and the crossover from heating to cooling occurs at a depth of 16 m. Above 16 m, the shortwave radiation transmitted through depth h is larger than the net surface heat flux. In the absence of buoyancy forcing from a freshwater flux, a mixed layer would adjust deeper than this crossover point merely due to hydrostatic instability and, as a result, would warm due to a positive net surface heat flux. Overplotted are the model heating rates against the mean model mixed-layer depth, as well as the heating rate from (4) against 0.5 h. The maximum heating rates of 0.11°C mo^{-1} occur at a mean mixed layer depth of 30 m. This agrees well with the maximum rates from (4). The model rates are smaller than the rates from (4) below 40 m and reach negative rates below 55 m. This deviation is due to entrainment of cold thermocline water, which is not accounted for in (4). To confirm this, the resulting SST rates from the 64 models runs ini-

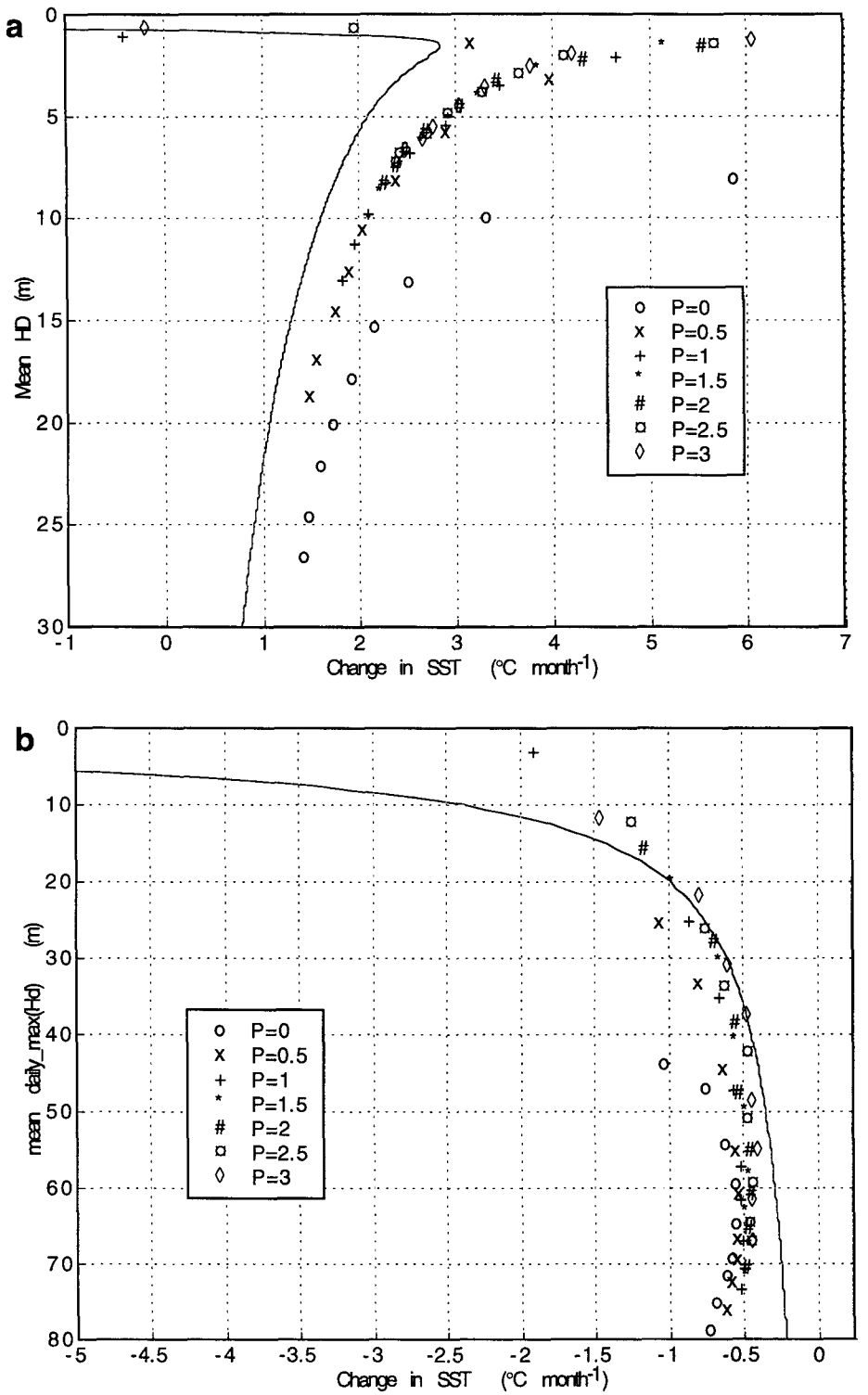

FIG. 14. Rate of SST warming as a function of mixed layer depth for low wind period and wind burst period. The idealized rate of warming (assuming no entrainment cooling) from the mean surface heat fluxes is plotted as a function of $0.5h$ (solid). The symbols are from the 64 model runs in which the rain was varied from zero to three times the observed and wind stress was varied from zero to four times the observed values. The period of (a) low wind speeds from 5–16 January 1993 and (b) the wind burst from 20 December 1992 to 4 January 1993.

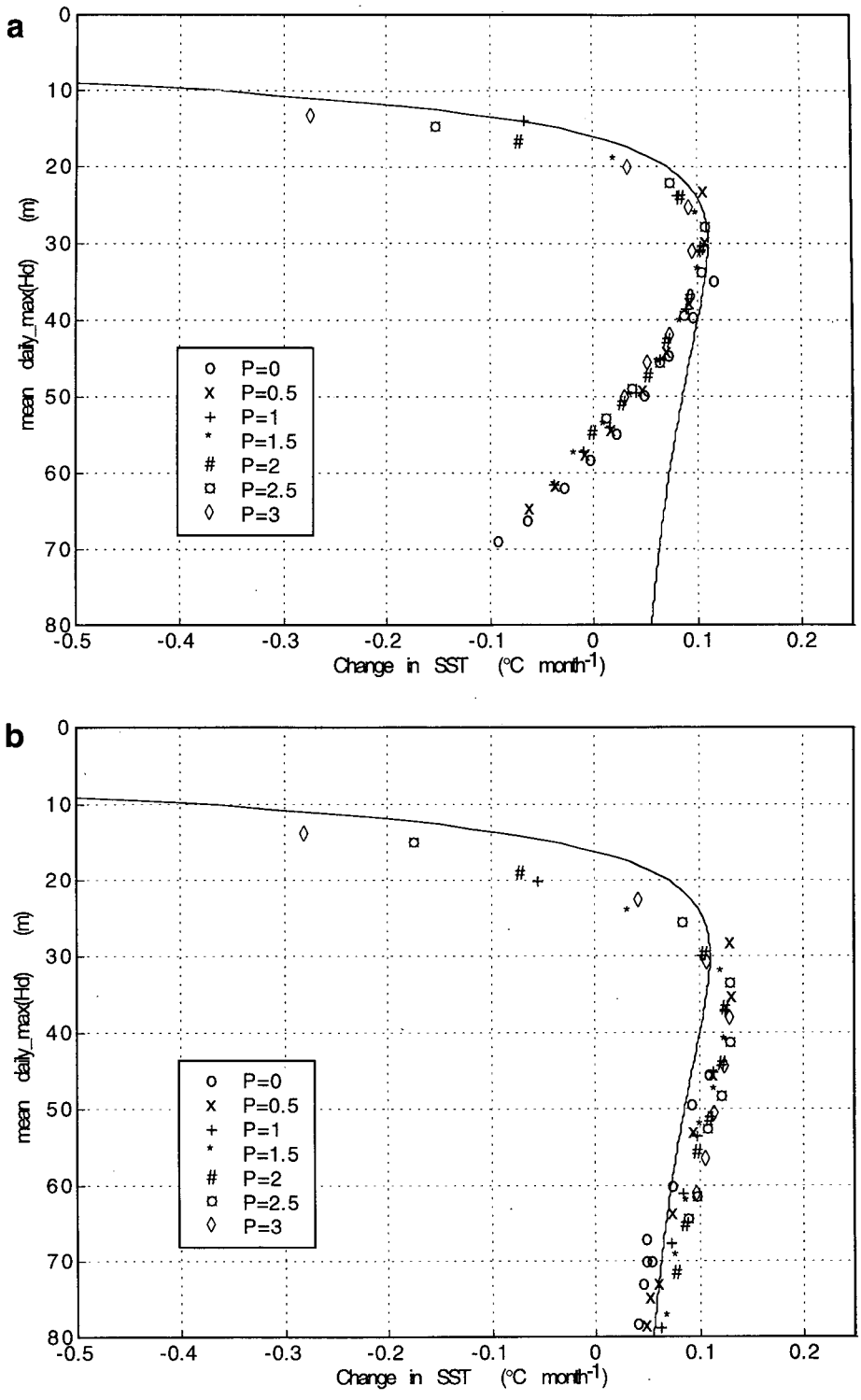

FIG. 15. Rate of SST warming as a function of mixed layer depth for the IOP mean. The idealized rate of warming (assuming no entrainment cooling) from the mean surface heat fluxes is plotted as a function of $0.5h$ (solid). The symbols are from 64 model runs in which the rain was varied from zero to three times the observed and wind stress was varied from zero to four times the observed values. The model runs were initialized with (a) the mean observed temperature and salinity profiles and (b) a constant temperature and salinity above 150 m. The effects of entrainment cooling on SST seen in (a) are absent in (b).

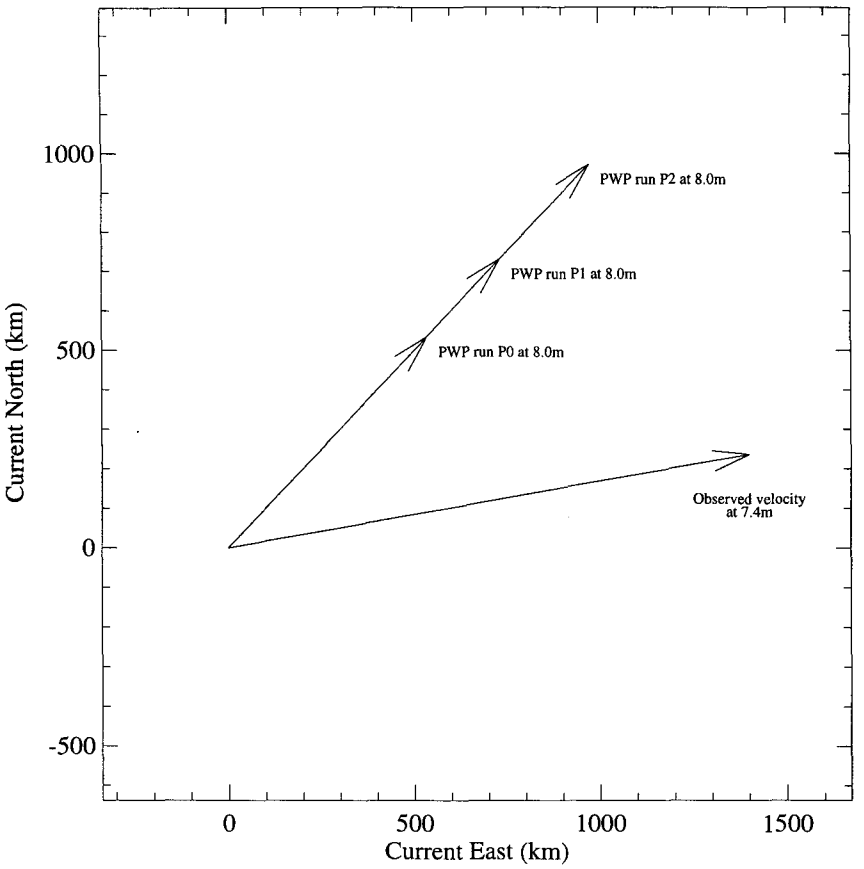

FIG. 16. The observed and modeled net surface displacement. The observed velocity record on the mooring at 7.4 m is integrated in time to calculate a net displacement. The same calculation is done using the model velocities at 8.0-m depth from three runs corresponding to increasing rain rates: P0 ($P = 0$), P1 (P_{obs}), and P2 ($2 \times P_{obs}$).

tialized with constant temperature and salinity to 150 m are shown in Fig. 15b. In this case, the SST is always warming when the mean mixed layer depth is below 20 m, and the rates are better matched to those from (4) below 50 m.

An abundance of precipitation in the model (or reduction in wind stress) leads to a shallow mixed layer that cools. The buoyant freshwater can limit the vertical mixing, allowing the surface waters to cool off and the deeper waters to warm, while maintaining hydrostatic stability. In the depth range from 20 to 50 m, the rate of temperature change is very sensitive to mixed layer depth. Run P1 has mixed layer depths that lie in the region where SST warming is at a maximum; P0 has deeper mixed layer depths by 10 m on average, and the net SST change is slightly smaller because of the larger effective volume to heat, as well as some entrainment cooling. In P2, the extra precipitation limits vertical mixing to the extent that the surface layer does not warm as rapidly since significant shortwave radiation is transmitted through the mixed layer base.

b. Surface velocities and buoyancy forcing

What is the effect of local precipitation, through its control of mixed layer depth, on the surface currents? A fresh buoyant surface layer will resist shear mixing and entrainment and accelerate rapidly in response to wind forcing. Progressive velocity vector diagrams provide an estimate of the net displacement of the surface waters, assuming a frozen field. The progressive vector diagram from the observed currents at 7.4 m indicates net eastward drift of 1500 km over the IOP (Fig. 16). This is an average surface current of 12.4 cm s^{-1}. The progressive vector diagram from model runs P0, P1, and P2 show net displacement toward the northeast (Fig. 16). The net eastward displacements are 525 km, 700 km, and 950 km, and average eastward currents are 4.3, 5.8, and 7.9 cm s^{-1} for runs P0, P1, and P2, respectively. This suggests that the shallower buoyant mixed layer that occurs with increased precipitation has larger mean wind-driven velocities. This is analogous to the "slippery near-surface layer," de-

scribed by Kudryavtsev and Soloviev (1990), that arises due to daytime solar heating.

8. Discussion

Previous studies, as well as the appendix presented here, clearly show that at times horizontal and vertical advection play an important role in the warm pool mixed layer dynamics. These "nonlocal" physical processes are not included in this analysis, but are clearly important on climatological timescales. However, previous tropical ocean modeling efforts that have included these nonlocal processes have not included the fine vertical and temporal resolution, the penetrating shortwave radiation, nor the accurate forcing fields used in this study. Weller and Anderson (1996) show that the surface forcing time series from the buoy are much more accurate and complete than available gridded products commonly used for driving the tropical ocean models. In addition, Weller and Anderson (1996) demonstrate that the observed upper-ocean variability over the IOP cannot be reproduced in a 1D model using gridded model fluxes from ECMWF while much of the variability is captured using the buoy fluxes. Thus, it is instructive to consider these unique, though limited, one-dimensional results in terms of ENSO timescale variations in the warm pool.

ENSO events recur approximately every 3 to 5 years, and it has been hypothesized that baroclinic Kelvin and Rossby waves, as modified by coupling with the atmosphere, are the primary mechanism by which the ocean remembers the last ENSO event (Mantua and Battisti 1994). This is the popular "delayed oscillator" theory. Webster and Lukas (1992) suggested an alternative mechanism. They hypothesized what might be termed the "capacitor" theory for ENSO, in which the annual net freshwater flux in the western Pacific acts to increase the stratification (and upper-ocean stability) and support the accumulation of heat. The greater heat content further tends to reduce the sensitivity of sea surface temperature to wind forcing, as well as insulating the sea surface from thermocline depth fluctuations associated with baroclinic waves. As the area and thickness of the warm pool increase, the atmospheric circulation regionally, including the Asian monsoons, is affected. An eastward displacement of the energetic Asian winter monsoon forcing over the warm pool ultimately results in the eastward displacement of the warm pool into the central Pacific and the discharge of the excess heat content that accumulates in the warm pool between ENSO events. Recently, Jin (1996, manuscript submitted to *J. Atmos. Sci.*) has developed analytical theory that includes both hypothesized mechanisms, which he terms the "discharge oscillator" theory.

Given the existence of the barrier layer and the small magnitude of the net positive mean surface heat flux, the weak average entrainment cooling needed to close the warm pool heat budget can be provided by relatively strong but infrequent mixing events, such as during episodic westerly wind bursts (Meyers et al. 1986). In the absence of such westerly wind bursts, the mixed layer can warm, thus charging the capacitor. This would imply that net cooling tends to occur most often during the onset of ENSO events, when westerly wind bursts are more frequent (Luther et al. 1983), and when the thermocline is shallower and more accessible to wind-driven mixing. A by-product of the westerly bursts is an eastward displacement of the warm pool, which may result from the buoyancy surface layer accelerating eastward and the lack of entrainment of cool thermocline water keeping the mixed layer waters relatively warm. This eastward movement of the warm pool effectively discharges the "capacitor," as these waters cannot directly return to the western Pacific along the equator because of the asymmetry associated with the rotation of the earth. In the long-term mean, there can be no continuing temperature increase of the mixed layer, but the ENSO phenomenon may exist solely because there is an inadequate removal of heat from the upper layer of the western tropical Pacific Ocean by the mean ocean circulation, as originally suggested by Wyrtki (1985).

As mentioned earlier, the IOP-mean BL thickness is substantially less than climatological estimates. This, we believe, is consistent with the capacitor hypothesis. First, although the rainfall (as estimated by outgoing longwave radiation) in the IFA during the IOP was not markedly anomalous (Gutzler et al. 1994), it had been dry compared to climatology throughout most of 1992. Second, the center of the warm pool (warmest SST and minimum OLR) was obviously displaced to the east of its climatological position during the IOP (Gutzler et al. 1994; Lukas et al. 1995). Thus, the warm pool discharge process had been ongoing for some time. The brief "recovery" of the warm pool noted by Lukas et al. (1995) was not long enough to recharge the heat content and rebuild the BL before the discharge process continued again during the IOP. Evidence of such variation in the BL thickness associated with ENSO was presented by Shinoda (1993).

The results from the 1D model analysis support three key parts of the "capacitor" theory. First, the large amount of precipitation does increase the buoyancy of the surface layer, decoupling it from the cooler thermocline below. Without the precipitation, the mixed layer would more often deepen and entrain cool water. Second, the balance between buoyancy forcing and wind stress observed in the warm pool results in a mixed layer depth such that the maximum heating of the surface layer can occur. Either increasing the precipitation or decreasing wind stress alone will lead to a shallower surface layer that warms more slowly due to the nature of shortwave radiation absorption in the mixed layer. Either decreasing precipitation or increasing wind stress alone will deepen the mixed layer and increase entrainment cooling. Third, holding the wind stress constant, the warm surface waters move more rapidly to the east with increasing precipita-

tion since the shallow buoyant fresh surface layer yields higher wind-driven velocity while resisting shear mixing and entrainment cooling.

The role of shortwave radiation penetrating through the base of the mixed layer (Lewis et al. 1990; Siegel et al. 1995) is important to the warm pool heat budget and deserves careful consideration. A thick barrier layer may limit mixed layer cooling by entrainment of cooler thermocline water, but the shallower mixed layer base would allow more shortwave radiation to pass through the mixed layer (thus warming the barrier layer). The relationship between mixed layer depth, surface buoyancy forcing, and penetrating radiation, together with the relatively small size of the mean net heat flux at the surface of the warm pool, gives rise to the possibility of an oceanic thermostat mechanism. The equilibrium mixed layer depth is given by the Monin–Obukhov length scale. Increasing precipitation increases the buoyancy flux, B, which reduces the Monin–Obukhov length scale L_b, but the flux of shortwave radiation through the base of the mixed layer increases, and a net cooling tendency in the mixed layer may result, which would support mixed layer deepening. Alternatively, reduced precipitation will lead toward a deeper mixed layer, which will trap more of the penetrating radiation and thus the mixed layer will tend to warm and shoal. The "set point" of this thermostat appears to be controlled by the mean rain rate.

Inclusion of the freshwater flux greatly improves the success of one-dimensional models in the warm pool. Some descrepencies between the 1D models and the observations remain after this improvement. The three-dimensional response of the upper ocean and its role in entrainment and advection is, of course, important and, most apparently, plays an important role in the mixed heat and salt budget during the westerly wind burst in December. However, insight has been gained here through the use of the 1D model. We have learned that further studies that incorporate spatial variability in the surface forcing and three-dimensional ocean dynamics should explicitly consider the roles that precipitation and penetrating shortwave radiation play in controlling the sea surface temperature.

9. Summary

A tendency was noted for 2-day-averaged freshwater and heat flux contributions to surface buoyancy forcing to be negatively correlated (-0.52), which helps to reduce the variance of the total buoyancy flux and, thus, the mixed layer depth. However, the variability of these components of the buoyancy flux results in a cycling between temperature and salinity control of the mixed layer depth, with implications for the mixed layer temperature and salinity. The barrier layer, which has been often observed in the warm pool, was present during limited portions of the COARE IOP, and the IOP-mean BL thickness is 9 m, substantially thinner than the climatological estimate of Sprintall and Tomczak (1992).

The heat and salt budgets for the upper 50 m over the entire IOP cannot be closed in a one-dimensional analysis. The largest deviation from this balance occurs during the strong westerly wind burst of December 1992. However, for significant portions of the record the one-dimensional budgets can be closed, suggesting the importance of local air–sea interactions in the maintenance of the warm pool. The net freshwater flux is of particular importance. Roughly half the time the depth of the mixed layer is controlled by vertical salinity gradients associated with heavy precipitation. One-dimensional mixed layer model experiments show that the freshwater flux during the early January recovery of SST, following the December westerly wind bursts, was important to the mixed layer heat budget and, therefore, to the rapid rise of SST after the burst. The primary impact of the buoyancy flux associated with the rainfall was to limit the depth of mixing, thus concentrating the heat near the surface and allowing for a larger warming trend.

The thermodynamically active hydrological cycle of the warm pool is important to the climate system. It has already been established that the atmosphere is quite sensitive to relatively small SST variations in the warm pool region; this work has shown that SST in this region is sensitive to changes in the air–sea heat fluxes because of the generally shallow mixed layer. This combination of sensitivity allows for stronger feedbacks between the atmosphere and the ocean (Sarachik 1978). The barrier layer, when it is present, also insulates the mixed layer from the cooler waters in the thermocline, minimizing the influence of adiabatic ocean dynamics on the warm pool SST. Thus, the inclusion of rainfall should result in a much stronger local coupling between the atmosphere and ocean in the warm pool region than is now found in coupled models, which do not have a complete and accurate simulation of the hydrologic cycle.

Acknowledgments. The deployment of the mooring was done in cooperation with A. Plueddemann (WHOI), who along with M. Tomczak (Flinders University of South Australia) contributed instrumentation to the mooring. Our work was funded by National Science Foundation Grants OCE91-10559 and OCE91-13948, and NASA Grant NAS5-31722 under the Earth Observing System program. Drs. M. McPhaden and C. Fairall provided precipitation data from the ATLAS and RV *Moana Wave*.

Stan Hayes made very early and quite substantial contributions to the planning of TOGA COARE. The development of the ATLAS buoy and the TOGA TAO array made it possible to conceive of an intensive large-scale process study such as COARE, while at the same time, the enhanced monitoring of the warm pool for TOGA COARE was important to the completion of the TAO array. The approach of making high quality ocean and atmospheric measurements from moored buoys has been demonstrated to be quite powerful for understand-

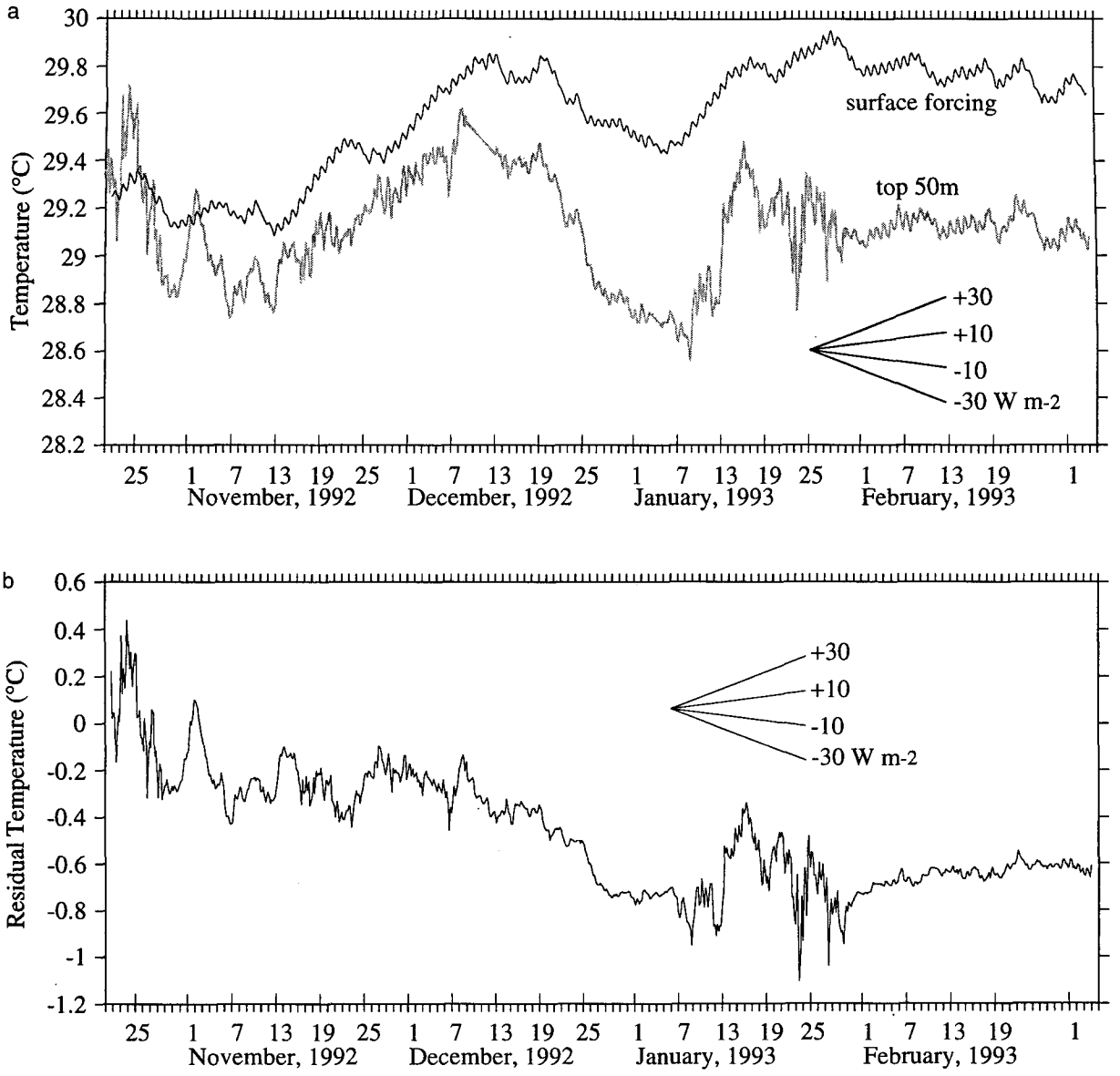

FIG. A1. Upper-ocean heat budget. The average temperature of the top 50 m (gray line) and the equivalent temperature if the surface heating was applied to this layer (black line) are plotted in (a). The difference between these two or the residual is shown in (b). The difference between these temperatures is due to advection, entrainment, and variability in the transmission of shortwave radiation at 50 m. The slopes for equivalent heating are given for reference.

ing the coupling of ocean–atmosphere. We are pleased to have this opportunity to dedicate this work to the memory of Stan Hayes.

APPENDIX

One-Dimensional Heat and Salt Budgets

To quantify the variability of the heat and salt content of the upper ocean, which can be accounted for by surface forcing alone, we examine the success of a one-dimensional budget. The heat budget is calculated for a constant depth layer, h, chosen to be 50 m. This depth is consistent with the maximum observed depth of the isopycnal layer. The heat budget, written in terms of a depth-averaged temperature, is

$$T_{\mathrm{mL}} - \left\{ \frac{1}{\rho C_p h} \int_0^t [Q_{\mathrm{lw}} + Q_{\mathrm{lat}} + Q_{\mathrm{sen}} + Q_{\mathrm{sw}}(1 - F(h)(h))]dt + T_0 \right\} = \delta T, \quad \text{(A1)}$$

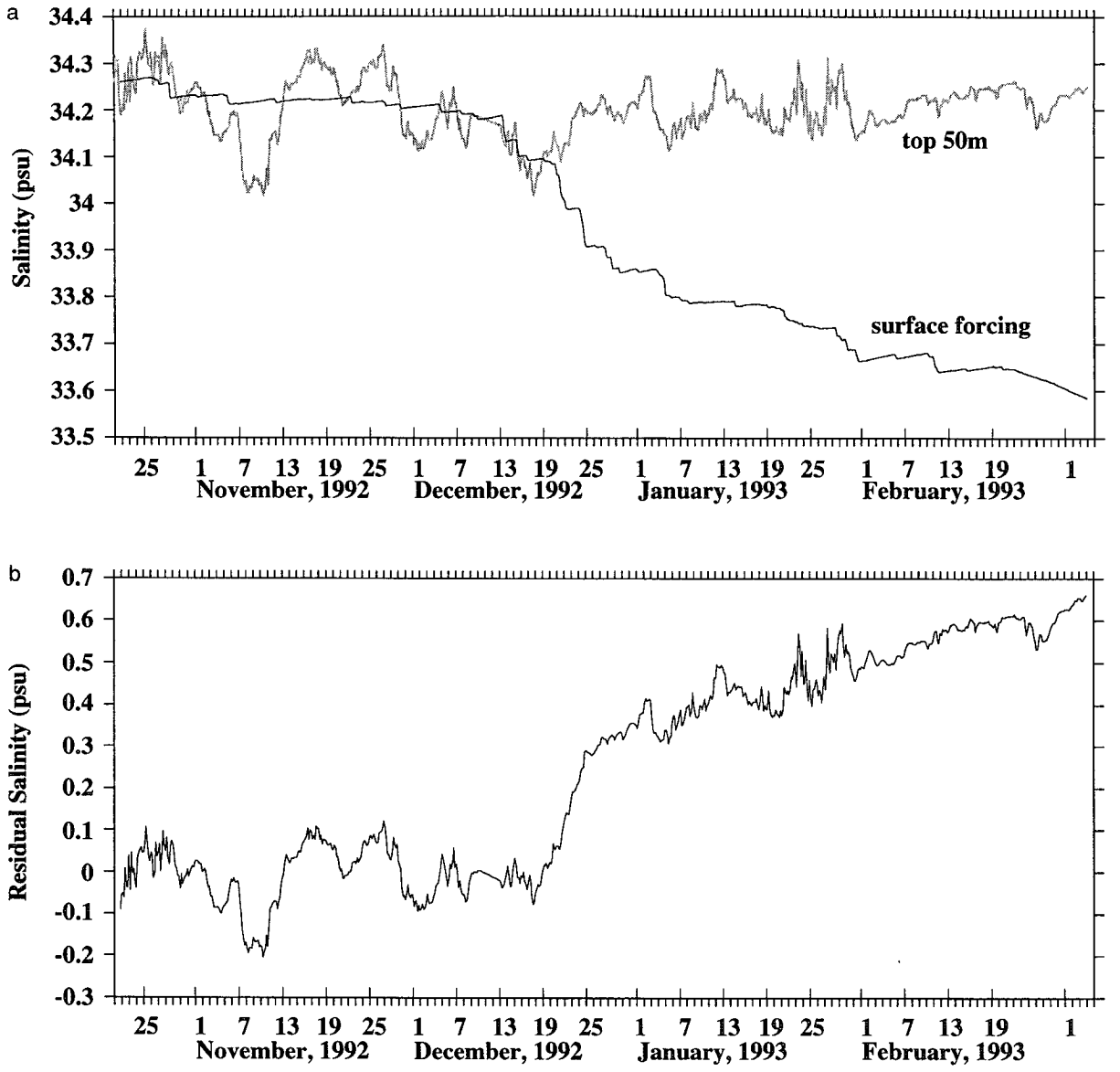

FIG. A2. Upper-ocean salt budget. The average salinity of the top 50 m (gray line) and the equivalent salinity if the surface freshwater fluxes were applied to this layer (black line) are plotted in (a). The difference between these two, or the residual, is shown in (b). The difference between these salinities is due to advection, entrainment, and errors in precipitation measurements.

were ρ and C_p are the density and heat capacity of water, respectively; F is the depth-averaged temperature of the layer; T_0 is the initial value of T_{mL}; and $F(h)$ is the shortwave transmission function. The importance of accounting for the penetrating solar radiation on the heat budget of the upper ocean in the equatorial Pacific was pointed out by Lewis et al. (1990). The residual term δT is all the temperature variability that cannot be accounted for by surface forcing and includes advection, mixing at the base of the layer, and variability in the shortwave transmission in the upper ocean. Siegel et al. (1995) report that transmission at 50 m varies from 5.5% to 2.7% in the IFA, as a result of a plankton bloom that occurred following the westerly wind burst in late December 1992. With the mean observed net surface shortwave of 194 W m^{-2}, the variability of transmission out the base of this layer is 5.5 W m^{-2}. Siegel et al. (1995) suggest a climatological value of 4.3% in the warm pool region for transmission through 50 m, which is employed in these calculations.

The first two terms from the heat budget and the residual are shown for the IOP in Fig. A1. The terms have been averaged over one hour before plotting. During the first 7 days there is a rapid change in the residual

value that corresponds to a rapid deepening of the thermocline from 50 to 100 m, perhaps due to a tropical cyclone that was in the area just prior to the deployment of the mooring. During November, the layer heat content and the surface forcing are in close balance during net heating of the upper ocean. There are some variations over 1 to 5 days in the heat content that occur during light wind periods that swamp any signal from the diurnal heating cycle. At the onset of the westerly wind burst in mid-December, the layer cools rapidly relative to the integrated surface forcing until the beginning of January 1993. There is again 1 to 5 day variability in the heat content associated with the low winds and shoaling of the thermocline during the last three weeks of January; however, the net change in heat content over this period is consistent with the surface forcing. During the month of February, the closest agreement between the surface forcing and upper ocean heat content is observed, with a slight warming of the upper ocean relative to the surface forcing, which corresponds to less than 5 W m^{-2}.

The salt budget is given by

$$S_{mL} - S_0\left(1 + h^{-1}\int_0^t (E - P)dt\right) = \delta S, \quad \text{(A2)}$$

were S_{mL} is the depth-average salinity; S_0 is the initial salinity of the layer; and E and P are the evaporation and precipitation rates, respectively. The evaporation is calculated from the latent heat flux. The residual salinity is δS, which includes all the advective and vertical mixing terms. Over the IOP, there is no net change in the observed salinity of the layer (Fig. A2). High-frequency variability in S_{ml} is observed during the same low wind periods in November and January that the variability of heat content was observed. During this period S_{mL} and T_{mL} are inversely correlated with a correlation coefficient of -0.85 from 6 to 29 January 1993. Large fluctuations in the layer salinity observed in November correspond to excursions in the pycnocline depth. The largest accumulation of precipitation occurs during the westerly wind bursts from 15 December 1992 to 3 January 1993. However, the actual variability in the layer salinity is relatively small during the westerly wind bursts. This lack of salinity response to westerly wind bursts is similar to that observed by Delcroix et al. (1993) in the warm pool during February–April 1991. This contrasts with the observed salinity response to westerly wind bursts in November 1989 when surface salinities in the warm pool fell by 1 psu after the onset of westerlies (McPhaden et al. 1992). Salt advection in the warm pool was also noted by Sprintall and McPhaden (1994). The layer salinity has the lowest variability during February 1993, corresponding to the time when the one-dimensional heat budget is closely balanced.

Over the whole IOP, the one-dimensional heat budget is closed to within 5–10 W m^{-2}. Imbalance of the magnitude could be due to shortcomings in our prescription of the absorption of shortwave radiation or to uncertainties of the surface heat fluxes. The imbalance of the salt budget, however, is large and importation of salt is required for closure. Additional vertical mixing would cool the warm pool as well as add salt, so it may be that horizontal advection was important to the salt budget. If the horizontal gradients in warm pool temperature are small relative to those of salinity, then horizontal advection could help close the salt budget without altering the heat budget.

REFERENCES

Bathen, K. H., 1972: On the seasonal changes in the depth of the mixed layer in the North Pacific Ocean. *J. Geophys. Res.*, **77,** 7138–7150.

Bradley, F., and R. Weller, 1995: *Proceedings of the Joint Workshop of the TOGA COARE Flux and Atmospheric Working Groups.* Boulder, CO, TOGA COARE International Project Office, 35 pp.

Chen, D., L. M. Rothstein, and A. J. Busalacchi, 1994: A hybrid mixing scheme and its application to tropical ocean models. *J. Phys. Oceanogr.*, **24,** 2156–2179.

Cornillon, P., and L. Stramma, 1985: The distribution of diurnal sea surface warming events in the western Sargasso Sea. *J. Geophys. Res.*, **90,** 11 811–11 815.

Delcroix, T., G. Eldin, M. McPhaden, and A. Morliere, 1993: Effects of westerly wind bursts upon the western equatorial Pacific Ocean, February–April 1991. *J. Geophys. Res.*, **98**(C9), 16 379–16 385.

Eriksen, C. C., 1993: Equatorial ocean response to rapidly translating wind bursts. *J. Phys. Oceanogr.*, **23,** 1208–1230.

Fairall, C. W., E. F. Bradley, J. S. Godfrey, G. A. Wick, J. B. Edson, and G. S. Young, 1996a: The cool skin and the warm layer in bulk flux calculations. *J. Geophys. Res.*, **101**(C1), 1295–1308.

——, ——, D. P. Rogers, J. B. Edson, and G. S. Young, 1996b: The TOGA COARE bulk flux algorithm. *J. Geophys. Res.*, **101**(C2), 3747–3764.

Flament, P., and M. Sawyer, 1995: Observations of the effect of rain temperature on the surface heat flux in the intertropical convergence zone. *J. Phys. Oceanogr.*, **25,** 413–419.

Gill, A. E., and E. M. Rasmusson, 1983: The 1982–83 climate anomaly in the equatorial Pacific. *Nature,* **306,** 229–234.

Godfrey, J. S., and E. Lindstrom, 1989: On the heat budget of the equatorial west Pacific surface mixed layer. *J. Geophys. Res.*, **94,** 8007–8017.

Gutzler, D. S., G. N. Kiladis, G. A. Meehl, K. M. Weickmann, and M. Wheeler, 1994: Seasonal climate summary: The global climate of December 1992–February 1993. Part II: Large-scale variability across the tropical Pacific during TOGA COARE. *J. Climate,* **7,** 1606–1622.

Hawkins, J. D., R. M. Clancy, and J. F. Price, 1993: Use of AVHRR data to verify a system for forecasting diurnal sea surface temperature variability. *Int. J. Remote Sens.*, **14,** 1347–1357.

Hayes, S. P., L. J. Mangum, J. Picaut, A. Sumi, and K. Takeuchi, 1991: TOGA-TAO: A moored array for real-time measurements in the tropical Pacific Ocean. *Bull. Amer. Meteor. Soc.*, **72,** 339–347.

Hosom, D. S., R. A. Weller, R. E. Payne, and K. E. Prada, 1995: The IMET (improved meteorology) ship and buoy system. *J. Atmos. Oceanic Technol.*, **12,** 527–540.

Jerlov, N. G., 1968: *Optical Oceanography.* Elsevier, 194 pp.

Kraus, E. B., and J. S. Turner, 1967: A one-dimensional model of the seasonal thermocline. II. The general theory and its consequences. *Tellus,* **19,** 98–105.

Kudryavstev, V. N., and A. V. Soloviev, 1990: Slipery near-surface layer of the ocean arising due to daytime solar heating. *J. Phys. Oceanogr.*, **20,** 617–627.

Lindstrom, E., R. Lukas, R. Fine, E. Firing, S. Godfrey, G. Meyers, and M. Tsuchiya, 1987: The Western Equatorial Pacific Ocean Circulation Study. *Nature,* **330,** 533–537.

Levitus, S., 1982: *Climatological Atlas of the World Ocean.* NOAA Prof. Paper No. 13, U.S. Govt. Printing Office, 173 pp.

Lewis, M. R., M. Carr, G. Feldman, W. Esaias, and C. McClain, 1990: Influence of penetrating solar radiation on the heat budget of the equatorial Pacific Ocean. *Nature,* **347,** 543–544.

Lukas, R., and E. Lindstrom, 1991: The mixed layer of the western equatorial Pacific Ocean. *J. Geophys. Res.,* **96**(suppl.), 3343–3357.

——, P. J. Webster, M. Ji, and A. Leetmaa, 1995: The large-scale context for the TOGA Coupled Ocean–Atmosphere Response Experiment. *Meteor. Atmos. Phys.,* **56,** 3–16.

Luther, D. S., D. E. Harrison, and R. A. Knox, 1983: Zonal winds in the central equatorial Pacific and El Niño. *Science,* **222,** 327–330.

Mantua, N. J., and D. S. Battisti, 1994: Evidence for the delayed oscillator mechanism for ENSO: The "observed" oceanic Kelvin mode in the far western Pacific. *J. Phys. Oceanogr.,* **24,** 691–699.

McPhaden, M., F. Bahr, Y. duPenhoat, E. Firing, S. Hayes, P. Niiler, P. Richardson, and J. Toole, 1992: The response of the western equatorial Pacific Ocean to westerly wind bursts during November 1989 and January 1990. *J. Geophys. Res.,* **97,** 14 289–14 303.

Mellor, G. L., and T. Yamada, 1982: Development of a turbulent closure model for geophysical fluid problems. *Rev. Geophys. Space Phys.,* **20,** 851–875.

Meyers, G., J.-R. Donguy, and R. K. Reed, 1986: Evaporative cooling of the western equatorial Pacific Ocean by anomalous winds. *Nature,* **323,** 523–526.

Niiler, P., and E. B. Kraus, 1977: One-dimensional models of the upper ocean. *Modelling and Prediction of the Upper Layers of the Ocean,* E. B. Kraus, Ed., Pergamon Press, 142–172.

——, and J. Stevenson, 1982: The heat budget of tropical ocean warm-water pools. *J. Mar. Res.,* **40**(Suppl.), 465–480.

Palmer, T. N., and D. A. Mansfield, 1984: Response of two atmospheric general circulation models to sea-surface temperature anomalies in the tropical east and west Pacific. *Nature,* **310,** 483–485.

Peters, H., and M. C. Gregg, 1987: Equatorial turbulence: Mixed layer and thermocline. *Proc. Aha Huliko'a Hawaiian Winter Workshop,* Honolulu, HI, University of Hawaii at Manoa, 25–45.

Price, J. F., C. Mooers, and J. van Leer, 1978: Observation and simulation of storm-induced mixed-layer deepening. *J. Phys. Oceanogr.,* **8,** 582–599.

——, R. Weller, and R. Pinkel, 1986: Diurnal cycling: Observations and models of upper ocean response to diurnal heating, cooling and wind mixing. *J. Geophys. Res.,* **91**(C7), 8411–8427.

Richards, K. J., M. E. Inall, and N. C. Wells, 1995: The diurnal mixed layer and upper ocean heat budget in the western equatorial pacific. *J. Geophys. Res.,* **100**(C4), 6865–6879.

Sarachik, E. S., 1978: Tropical sea surface temperature: An interactive one-dimensional atmosphere–ocean model. *Dyn. Atmos. Oceans,* **2,** 455–469.

Schudlich, R. R., and J. F. Price, 1992: Diurnal cycles of current, temperature, and turbulent dissipation in a model of the equatorial upper ocean. *J. Geophys. Res.,* **97**(C4), 5409–5422.

Shinoda, T., 1993: Variation of the thermohaline structure in the western equatorial Pacific upper ocean. Ph.D. dissertation, University of Hawaii at Manoa, 190 pp.

——, and R. Lukas, 1995: Lagrangian mixed layer modeling of the western equatorial Pacific. *J. Geophys. Res.,* **100**(C2), 2523–2541.

Siegel, D. A., J. C. Ohlmann, L. Washburn, R. R. Bidigare, C. T. Noose, E. Fields, and Y. Zhou, 1995: Solar radiation, phytoplankton pigments and the radiant heating of the equatorial Pacific warm pool. *J. Geophys. Res.,* **100**(C3), 4885–4891.

Sprintall, J., and M. Tomczak, 1992: Evidence of the barrier layer in the surface layer of the Tropics. *J. Geophys. Res.,* **97**(C5), 7305–7316.

——, and M. McPhaden, 1994: Surface layer variations observed in multiyear time series measurements from the western equatorial Pacific. *J. Geophys. Res.,* **99**(C1), 963–979.

Webster, P. J., and R. Lukas, 1992: TOGA COARE: The Coupled Ocean–Atmosphere Response Experiment. *Bull. Amer. Meteor. Soc.,* **73,** 1377–1416.

Weller, R. A., and S. P. Anderson, 1996: Surface meteorology and air–sea fluxes in the western equatorial Pacific warm pool during TOGA COARE. *J. Climate,* **9,** 1959–1990.

——, D. L. Rudnick, R. E. Payne, J. P. Dean, N. J. Pennington, and R. P. Trask, 1990: Measuring near-surface meteorology over the ocean from an array of surface moorings in the subtropical convergence zone. *J. Atmos. Oceanic. Technol.,* **7,** 85–103.

Woods, J. D., 1980: Diurnal and seasonal variation of convection in the wind-mixed layer of the ocean. *Quart. J. Roy. Meteor. Soc.,* **106,** 379–394.

Wyrtki, K., 1985: Water displacements in the Pacific and the genesis of El Niño cycles. *J. Geophys. Res.,* **90**(C7), 7129–7132.

Zhang, Q., 1995: The oceanic response to atmospheric forcing in the western equatorial Pacific. Ph.D. thesis, University of Rhode Island, 164 pp.